A High Fat Diet during Mouse Pregnancy and Lactation targets GIP-regulated Metabolic Pathways in Adult Male Offspring.

Running title: GIPR knockout mice and fetal programming

Michael Kruse[1,2,5,#], Farnaz Keyhani-Nejad[1,2,5,#], Frank Isken[1,2,5], Barbara Nitz[3,4,5], Anja Kretschmer[3,4], Eva Reischl[3,4], Tonia de las Heras Gala[4], Martin A. Osterhoff[1,2,5], Harald Grallert[3,4,5], Andreas F. H. Pfeiffer[1,2,5*]

[1]Department of Clinical Nutrition, German Institute of Human Nutrition, Nuthetal, Germany;
[2]Department for Endocrinology, Diabetes and Nutrition, Charité – University of Medicine, Berlin, Germany.
[3]Research Unit of Molecular Epidemiology, Helmholtz Zentrum München, German Research Center for Environmental Health, Neuherberg, Germany
[4]Institute of Epidemiology II, Helmholtz Zentrum München, German Research Center for Environmental Health, Neuherberg, Germany
[5]German Center for Diabetes Research

[#]Equal contribution
*Corresponding author:
Andreas F. H. Pfeiffer, MD, PhD
Department of Clinical Nutrition
German Institute of Human Nutrition
Arthur-Scheunert-Allee 114-116
14558 Nuthetal, Germany
Phone: +49 33 200 88 2771
Fax: +49 33 200 88 2777
Email: afhp@dife.de

Word count: 3,998
Number of tables: 1
Number of figures: 7

Diabetes Publish Ahead of Print, published online December 2, 2015

ABSTRACT

Maternal obesity is a worldwide problem associated with increased risk of metabolic diseases in the offspring. Genetic deletion of the Gastric Inhibitory Polypeptide Receptor (GIPR) prevents high fat diet induced obesity in mice due to specific changes in energy and fat cell metabolism. We investigated whether GIP-associated pathways may be targeted by fetal programming and mimicked the situation by exposing pregnant mice to control or high fat diet (HFD) during pregnancy (IU) and lactation (L). Male wild type (WT) and *Gipr*$^{-/-}$ offspring received control chow until 25 weeks of age followed by 20 weeks of HFD. *Gipr*$^{-/-}$ offspring of mice exposed to HFD during IU/L became insulin resistant, obese, exhibited increased adipose tissue inflammation and decreased peripheral tissue substrate utilization after being re-introduced to HFD similar to WT mice on regular chow during IU/L. They showed decreased hypothalamic insulin sensitivity compared to *Gipr*$^{-/-}$ mice on control diet during IU/L. DNA-methylation analysis revealed increased methylation of CpG-dinucleotides and differential transcription factor binding of promoter regions of genes involved in lipid oxidation in muscle of *Gipr*$^{-/-}$ offspring on HFD during IU/L which were inversely correlated with gene expression levels. Our data identify GIP-regulated metabolic pathways that are targeted by fetal programming.

Gastric inhibitory polypeptide (GIP) is released from the duodenum after nutrient intake and regulates post-prandial insulin secretion (1). GIP is known for its anabolic effects in adipocytes (2) and has been shown to stimulate the activity of lipoprotein lipase in adipose tissue *in vitro* (3) (4). Genetic ablation of the GIP receptor (GIPR) protects from high fat diet (HFD) induced obesity and insulin resistance in mice (5). GIPR knockout (*Gipr*$^{-/-}$) mice use fat as energy substrate rather than storing it in adipocytes. Moreover, central appetite regulating pathways are down regulated in ovariectomized female *Gipr*$^{-/-}$ mice (6) and energy expenditure is increased in *Gipr*$^{-/-}$ mice exposed to a high glycemic index (7) or a high fat (8) diet.

Since *Gipr*$^{-/-}$ mice are protected from obesity when exposed to a post-weaning HFD, we hypothesized, that this phenotype may be lost when these mice were exposed to the same HFD during pregnancy (IU) and lactation (L). The *intra uterine* milieu has a persisting influence on the development of adult diseases (9) (10). Maternal caloric malnutrition as well as over nutrition during IU and L can induce metabolic disturbances later in life in offspring (11) (12). Animal studies have shown that mice exposed to a maternal HFD during IU/L and weaned onto a standard chow developed adiposity, insulin resistance and hepatosteatosis later in life (13) (14). Not only the diet during IU/L, but also the post-weaning diet is important for the manifestation of metabolic diseases. Studies investigating the interaction of a HFD during IU/L and post-weaning usually apply the HFD continuously from pre-mating throughout the end of the study in adulthood. However, in terms of programming effects of metabolic diseases studies investigating a "second hit" later in life (e. g. a HFD) after a time frame of regular diet might better reflect the adult onset of obesity as shown recently (15). Recent work suggests that the *intra uterine* milieu induces epigenetic alterations, such as DNA-methylation and histone modifications, which affect gene transcription that persists life-long (16). Pathways targeted by epigenetic programming are

of eminent importance to develop strategies reducing the metabolic risks faced by offspring of obese mothers. We therefore chose a model in which extensive research has already identified some pathways involved in the protection from obesity, the *Gipr*$^{-/-}$ mouse.

Our results demonstrate that *Gipr*$^{-/-}$ mice exposed to a HFD during IU/L, weaned onto a regular chow for 22 weeks and then re-exposed to the HFD lose their metabolic protection which is associated with hyper-methylation of certain CpG-dinucleotides in the promoter regions of genes involved in energy balance and with changes in central insulin sensitivity. This phenotype was similar to wild type mice which were exposed to a control chow during IU/L, but also challenged with a HFD later in life. We therefore conclude that the protection from diet induced obesity in *Gipr*$^{-/-}$ mice is "overruled" by deleterious and persistent fetal programming effects of a HFD up to at least 45 weeks of life and identify metabolic pathways addressed by GIP.

RESEARCH DESIGN AND METHODS

Animals and experimental design

Animals were maintained on a 12 hour light-dark cycle with *ad libitum* access to chow and water. Age- and body weight (BW) matched female mice heterozygote for the GIP receptor (*Gipr*$^{+/-}$) on a C57BL/6 background were maintained on either a control diet D12450B ("C": 10 kcal-% fat as soybean oil and lard, 20 kcal-% protein, 70 kcal-% carbohydrate, 3.85 kcal/g) or a high fat diet D12492 ("HFD": 60 kcal-% fat as soybean oil and lard, 20 kcal-% protein, 20 kcal-% carbohydrate, 5.24 kcal/g) 2 weeks prior to mating with a male *Gipr*$^{+/-}$ mouse and throughout pregnancy (IU) and lactation (L) (all diets from Research Diets, Inc., New Brunswick, USA). Offspring were genotyped at two to three weeks of life. Male *Gipr*$^{-/-}$ offspring on C diet or HFD during IU/L and WT offspring on C diet during IU/L were individually housed and placed onto C diet at postnatal day 21 and kept on this diet until the age of 25 weeks, followed by further 20 weeks on HFD. This resulted in *Gipr*$^{-/-}$ mice exposed to C during IU/L and to HFD at the age of 25 weeks (**KO C-C-H**), *Gipr*$^{-/-}$ mice exposed to HFD during IU/L and to HFD at the age of 25 weeks (**KO H-C-H**) and WT mice exposed to C during IU/L and to HFD at the age of 25 weeks (**WT C-C-H**). Results obtained for these groups during the first 25 weeks of life are indicated with the first two diet symbols (KO C-C, KO H-C and WT C-C). At the age of 45 weeks mice were sacrificed using cervical dislocation. Tissues were harvested, immediately frozen in liquid nitrogen and stored at -80°C. Fig. 1 illustrates the study design. Animal protocols were approved by the local governmental animal ethic review board (State of Brandenburg).

Biochemical measurements

Fasting blood samples were collected after an overnight fast at 45 weeks of age from the submandibular vein plexus. Serum glucose, triglycerides, total cholesterol and non-esterified fatty

acids (NEFA) were measured using commercial kits (glucose HK 125; triglycerides, total cholesterol: ABX Pentra, Monpellier, France; Wako, Germany) by using an autoanalyzer (Cobas Mira S, Hoffmann La Roche, Switzerland). Plasma insulin levels were determined as described previously (17).

Body weight and cumulative food intake

Body weight (BW) and cumulative food intake were measured weekly. Food consumption was expressed in kcal/g BW for the indicated age.

***Intra peritoneal (i. p.)* glucose tolerance test**

A glucose tolerance test (GTT) was performed at the age of 43 weeks. Overnight fasted mice received an i. p. injection of D-(+)-glucose (2.0g/kg BW) (18). Blood was taken from the submandibular vein plexus and added to heparinized collecting tubes for plasma glucose and insulin measurements at 0, 10, 30, 60 and 120 min after glucose injection.

Body composition

Body composition was determined by nuclear magnetic resonance spectroscopy (Mini Spect MQ 10 NMR Analyser, Bruker, Karlsruhe, Germany) in conscious mice (6) at the age of 13, 22, 31 and 42 weeks of life.

Quantitative real time-PCR analysis

mRNA expression was performed in epididymal white adipose tissue, gastrocnemius muscle and hypothalamus as previously described (19) (6). The hypothalamus was dissected as a whole without any further subfractionation. Primers were designed using Primer Express software

(Applied Biosystems). Primer sequences are listed in Supplementary Table 1. The constitutive gene HPRT was used as a housekeeping gene.

Hypothalamic insulin signaling

The hypothalamic insulin signaling pathway was analyzed by performing the PathScan® Intracellular Signaling Array Kit (Cell Signaling Technology, Danvers, MA, USA) that allows a quantitative analysis of the phosphorylation status of key proteins involved in insulin and energy signaling. 75 µl of total protein lysate was processed following the manufacturer's instructions. Signal density was visualized using LI-COR® Biosciences Odyssey® (LI-COR Bioscience, Bad Homburg, Germany).

Histology of white adipose tissue

Tissue was fixed in 10% buffered formalin, embedded in paraffin, sectioned at 5 µm and stained with hematoxylin and eosin. Adipocyte size was measured using CellProfiler 2.0 (www.cellprofiler.org). One visual field with at least forty cells of three samples of epididymal adipose tissue from one animal was analyzed for cell surface size and expressed in µm². The average adipocyte cell size for each group was calculated and the frequency of cells sizes sorted by categories was determined for each group.

For evaluating crown-like structures 2 µm sections were dewaxed using 3% hydrogen peroxide and incubated overnight (4°C) with an F4/80 anti-mouse antibody (1:8000, Serotec, Puchheim, Germany), followed by an anti-rat secondary antibody for mouse tissue that includes Histofine (Nichirei, Biosciences INC, Tokyo, Japan). Images were acquired by Mirax slide scanner (Carl Zeiss, Göttingen, Germany). Crown-like structures were determined in three randomly chosen areas within the slides.

DNA-methylation analysis

DNA extraction. Genomic DNA was extracted from muscle and hypothalamus using a commercial kit (Machery-Nagel, Dueren, Germany) following the manufacturer's protocol and quality was checked using a NanoDrop® ND-1000 Spectrophotometer (PEQLAB, Erlangen, Germany).

Sodium bisulfite modification. Genomic DNA (700-1000 ng) was bisulfite-treated using the EZ-96 DNA Methylation Kit (Zymo Research, Orange, CA, USA) according to the manufacturer's protocol.

DNA methylation analysis by mass spectrometry. Methylation was determined for five loci by MALDI-TOF mass spectrometry using EpiTYPER by MassARRAY (Sequenom, San Diego, CA) as previously described (20) (21). Briefly, the target regions were amplified from bisulfite-treated DNA in duplicate PCR reactions. Primers were designed using the SequenomEpiDesigner web resource (http://www.epidesigner.com). Primer sequences for all amplicons are listed in Supplementary Table 2. Methylation data were generated by the MassARRAY EpiTYPER v1.2 software (Sequenom).

Four samples were measured in duplicate for four amplicons. Quality control of the data was performed using EPITyper and the statistical software R (version 3.0.2) eliminating all samples and all CpG sites with a call rate lower than 80 %, respectively. In total 182 CpG-dinucleotides were measured (single sites and composite sites with two or more adjacent CpG sites falling within one analyzed fragment). CpG-dinucleotides relevant for this study are named regarding their distance to the transcription start site.

Electrophoretic mobility shift assays (EMSA)

Myoblast nuclear extracts from mouse C2C12 cells (Active Motif, #36078) were used for EMSA. Cy5-labelled and unlabeled oligonucleotides (Metabion) containing the methylated or unmethylated CpG from respective EpiTYPER experiments (Supplementary Table 3) were annealed and purified in a 12 % polyacrylamide gel. Binding reaction was carried out with or without different concentrations of unlabeled competitor oligonucleotides. In each reaction 6.5 µg of nuclear extract was incubated in 5x binding buffer (4 % v/v Glycerol, 1 mM $MgCl_2$, 0.5 mM EDTA, 0.5 mM DTT, 50 mM NaCl, 10 mM TrisHCl pH7.5) with 0.5 µg poly dI-dC (Roche Diagnostics) and 1 ng of labeled probe in a total volume of 10 µl for 25 min at 4°C. Protein-DNA complexes were separated on a 5.3 % polyacrylamide gel by electrophoresis in 0.5 x tris-borate-EDTA (TBE) running buffer. The gels were visualized by scanning with the Thyphoon Trio + Imager (GE Healthcare).

Data analysis

Data are represented by mean ± SEM. Statistical analyses were performed using one-way ANOVA with Tukey post hoc test (IBM SPSS 20, Chicago, USA). Data were tested for normal distribution. Non-normally distributed data were transformed to the logarithmic form to approximate the normal distribution.

Statistical analysis on methylation data was performed using R (version 3.0.2). For DNA-methylation analysis inferential statistics was used to analyze the 182 CpG sites of the three groups. For inferential statistics Student's t-test was performed and resulting p-values were adjusted for multiple testing. For descriptive analysis quotients of mean values from each two groups were calculated. For verification we also performed a correlation analysis of methylation data and gene expression data.

RESULTS

Body weight, body composition, food intake and serum lipids

During the first 25 weeks of life BW was not different except for week 4, 13 and 14 when KO H-C was heavier than KO C-C (Fig. 2A). When a HFD was fed at week 25 of life, KO C-C-H showed a significantly lower increase in BW than WT C-C-H (Fig. 2B). BW of KO H-C-H was in between the range of WT C-C-H and KO C-C-H. Before exposure to the HFD, adiposity of KO C-C was significantly lower compared to WT C-C (Fig. 2C). After 12 weeks on the HFD, KO C-C-H showed a significant decrease in adiposity compared to WT C-C-H, but now KO H-C-H had significantly increased adiposity compared to KO C-C-H, similar to WT C-C-H.

When offspring were on a regular diet, there was no difference in cumulative food intake for all groups at the age of 25 weeks (Fig. 2D). When mice were fed a HFD, KO C-C-H consumed significantly more kcal per g BW than WT C-C-H. In KO H-C-H there was a significant decrease in cumulative energy consumption compared to KO C-C-H which was similar to the level of WT C-C-H. Despite increased food intake, KO C-C-H had significantly reduced serum levels for total cholesterol compared to WT C-C-H (3.33±0.33 vs. 5.22±0.26 mmo/l, respectively, $P<0.005$) (Table 1). In KO H-C-H total cholesterol levels were 4.44±0.40 mmol/l, but this level was not significantly different compared to KO C-C-H. Serum levels for triglycerides and NEFA were unchanged.

KO H-C-H mice have decreased glucose tolerance

The i. p. GTT after 18 weeks on HFD showed that KO C-C-H had significantly lower fasting blood glucose levels compared to WT C-C-H (Fig. 3A and Table 1). However, KO H-C-H showed significantly increased fasting blood glucose levels compared to KO C-C-H ($P<0.05$) reaching similar levels like WT C-C-H. Accordingly, KO C-C-H had significantly lower fasting

insulin levels compared to WT C-C-H (P<0.05) (Table 1). KO H-C-H showed severe glucose intolerance like WT C-C-H (Fig. 3A). KO C-C-H, however, had significantly lower glucose levels after 30 min (P<0.05 and P<0.005 compared to KO H-C-H and WT C-C-H, respectively) and after 90 min (P<0.05 compared to KO H-C-H and WT C-C-H). Additionally, the AUC for glucose (Fig. 3B) was lower in KO C-C-H compared to WT C-C-H (P<0.05), but increased again in KO H-C-H (P<0.05 compared to KO C-C-H, P=n.s. compared to WT C-C-H). During the i. p. GTT *Gipr*$^{-/-}$ mice showed slightly lower insulin levels compared to WT with no significant difference between KO C-C-H and KO H-C-H (Fig. 3 C, D).

Increased adipocyte size in KO H-C-H mice

KO C-C-H had significantly smaller adipocytes compared to WT C-C-H (P<0.001, Fig. 4 A, C, D). HFD during IU/L caused an increase in adipocyte size in KO H-C-H (P<0.001 compared to KO C-C-H) (Fig. 4 A, D, E). Fig. 4B shows that KO C-C-H had more small adipocytes (< 2,000 μm²) compared to KO H-C-H and WT C-C-H, which both had more cell counts in categories with large adipocytes (≥ 8,000 μm²).

KO H-C-H mice exhibit increased markers of macrophage infiltration in white adipose tissue

Ccl2 mRNA expression was 48% decreased in KO C-C-H compared to WT C-C-H mice (P<0.05) (Fig. 5A). However, in KO H-C-H *Ccl2* mRNA expression was increased 2.73-fold compared to KO C-C-H (P<0.05). *Ccl3* mRNA levels were significantly down regulated by 43% in KO C-C-H (P<0.05 compared to WT C-C-H), and again 1.39-fold up regulated in KO H-C-H compared to KO C-C-H, however not significant. The same pattern was observed for mRNA expression of *Emr1*: It was decreased by 44% in KO C-C-H compared to WT C-C-H (P<0.05)

and 1.35-fold up regulated in KO H-C-H (P= n.s. compared to KO H-C-H). However, we could not detect differences in crown-like stuctures (Supplementary Figure 1). There was no difference in gene expression for *Tnf* and *Il6*.

KO H-C-H mice show a strong decrease of key genes of fatty acid oxidation in muscle compared to KO C-C-H mice

A strong increase in gene expression levels of *Ppara* (2.45-fold, P<0.01), *Ppargc1a* (1.78-fold, P<0.01), *Cpt1a* (1.39-fold, P<0.05) and *Cpt1b* (1.53-fold, P<0.01) was observed in KO C-C-H compared to WT C-C-H (Fig. 5B). This increase was abolished when *Gipr*$^{-/-}$ mice were exposed to a HFD during IU/L (KO H-C-H). These mice had the same gene expression levels as WT C-C-H. We did not observe any significant difference in gene expression for *Cd36*, *Lpl*, *Acadm* and *Acadl*.

Increased gene expression of phosphatidylinositol 3-kinase regulatory subunit p85α in the hypothalamus in KO H-C-H mice

In KO C-C-H hypothalamic gene expression of PI3K-p85α (*Pik3r1*) was 22% down regulated compared to WT C-C-H (P<0.01) (Fig. 6A), however, was again up-regulated in KO H-C-H similar to WT C-C-H. Phosphorylation of hypothalamic Akt at Thr308 or Ser473 was not significantly different between the groups (Fig. 6B). For phosphorylation of mTOR at Ser2448 a down regulation of 18% (P<0.05) was observed in KO C-C-H compared to WT C-C-H, that was again upregulated in KO H-C-H similar to the level of WT C-C-H. A similar regulation was observed for the phosphorylation of S6 at Ser235/236.

Gene expression of *Npy* was 1.27-fold up regulated and of *Lepr* was 32% down regulated in KO H-C-H compared to KO C-C-H (both $P<0.05$). There were no significant changes in expression for other anorexigenic and orexigenic genes (Supplementary Figure 2).

Altered promoter-methylation causes differential transcription factor binding at the *Ppara* promoter in muscle

DNA-methylation analyses were performed for the promoter regions of *Ppara*, *Ppargc1a*, *Cpt1b* and *Cpt1a* in muscle and for the promoter region of *Pik3r1* in hypothalamus. For *Cpt1b* we identified three CpG-sites ($CpG_{+227/224}$, CpG_{-72}, CpG_{-202}) that had a loss in DNA-methylation in KO C-C-H compared to WT C-C-H (Fig. 7A-C). In KO H-C-H methylation was again increased as seen in WT C-C-H. These changes in methylation were significantly inversely correlated with gene expression levels of *Cpt1b* ($r = -0.540$ for $CpG_{+227/224}$, $P<0.05$; $r = -0.593$ for CpG_{-72}, $P<0.05$; $r = -0.629$ for CpG_{-202}, $P<0.005$). For *Ppara* we identified one CpG-site at CpG_{-140} (Fig. 7D) that also showed a significant inverse correlation with gene expression levels ($r = -0.658$, $P<0.005$). We did not see any significant changes in DNA-methylation for the promoter of *Ppargc1a* or *Cpt1a* in muscle or of *Pik3r1* in hypothalamus. To identify the biological relevance of DNA methylation at the associated CpG-sites, EMSA were performed. We detected methylation specific binding of transcription factors at the *Ppara* promoter region using nuclear extracts from C2C12 mouse myoblasts in four independent EMSA. We observed additional protein-DNA-complex formation at the methylated *Ppara* CpG_{-140} site (Fig. 7E). For the other three tested CpG sites no methylation specific protein-DNA was detected (Supplementary Figures 3-5).

DISCUSSION

This study shows that *Gipr*$^{-/-}$ mice are no longer protected from the adverse effects of a HFD in early adulthood when this diet was applied during pregnancy (IU) and lactation (L). The phenotypic alterations were evident by increased adiposity, enlarged adipocytes, impaired glucose tolerance and increased pro-inflammatory gene expression in adipose tissue in KO H-C-H compared to KO C-C-H mice. KO H-C-H mice behaved like WT mice on a normal chow during IU/L and exposed to a HFD later in life. Mechanistically, this phenotype is most likely due to central inhibition of phosphatidylinositol 3-kinase causing decreased insulin sensitivity in the hypothalamus and to decreased peripheral fatty acid oxidation in skeletal muscle. Moreover, our study suggests that alterations in DNA-methylation might be at least partially responsible for the changes in energy consumption. WT mice on HFD during IU/L and re-exposed to this diet later in life (WT H-C-H) showed a similar metabolic phenotype like WT C-C-H. Results are shown in Supplementary Figures 6-11).

We did not see a relevant difference in body weight or body fat between KO H-C and KO C-C mice up to the age of 25 weeks. After starting the HFD at the age of 25 weeks, differences for genotypes and maternal diet became evident. KO C-C-H showed significantly lower body weight and total body fat compared to WT C-C-H as shown previously (5) (8). The growth curve of KO H-C-H mice was in between the WT C-C-H and KO C-C-H mice, but KO H-C-H mice had significantly increased total body fat after 6 and 12 weeks upon re-exposure to a HFD compared to KO C-C-H mice. We show that even after a time window of 22 weeks on C diet, *Gipr*$^{-/-}$ mice on a HFD during IU/L (“first hit”) are programmed to overreact towards the ”second hit” of the HFD compared to *Gipr*$^{-/-}$ mice on a C diet during IU/L. This is also reflected by the increased size of adipocytes in KO H-C-H compared to KO C-C-H mice, which is important, since the size of adipocytes is correlated with adipose tissue dysfunction and insulin resistance

(22). This strong programming phenomenon was shown recently in a CID1 mouse model (15): WT male offspring of damns fed a HFD during IU/L were kept on normal chow after weaning until the age of 25 weeks and then reintroduced to the HFD for 19 weeks. These mice showed higher BW, larger adipocytes and reduced glucose tolerance compared to mice exposed to the HFD at 25 weeks of age, only.

The GIP signaling pathway is necessary for adipocyte development (23). This might explain why lacking the GIPR protects *Gipr*$^{-/-}$ mice from diet induced obesity (5) (24). However, if the HFD appears as a "second hit" later in life, this protection disappears and the fetal programming effect of a HFD overrules the *Gipr*$^{-/-}$ phenotype. Nevertheless, there was less weight gain in the KO H-C-H mice than in WT controls suggesting that some protection remained despite fetal programming effects of a HFD. One possible component might relate to the moderate impairment of insulin release in the *Gipr*$^{-/-}$ mice which reduces the obesogenic effect of insulin. It is most likely that KO H-C-H as well as WT C-C-H mice have severe beta cell damage, since serum insulin concentrations were dramatically reduced during the i. p. GTT, whereas KO C-C-H were able to minimally increase insulin release at the beginning of the i. p. GTT.

Obesity is associated with increased gene expression of pro-inflammatory cytokines or monocyte chemoattractant protein-1 (MCP-1) (25). MCP-1 seems to be responsible for macrophage infiltration in adipose tissue (26) (27). Macrophage infiltration can be quantified by measuring gene expression of macrophage inflammatory protein 1-α (*Ccl3*) and *Emr1* (28) (29). We saw a significant decrease of gene expression of *Clc2*, *Ccl3* and *Emr1* in KO C-C-H compared to WT C-C-H. In KO H-C-H, gene expression of *Clc2* significantly increased, whereas for *Emr1* and *Ccl3* there was a trend for up-regulated gene expression in these mice.

Even though the GIPR is absent in skeletal muscle (30) (31), genes involved in fatty acid oxidation were significantly up-regulated in KO C-C-H compared to WT C-C-H, but were down regulated in KO H-C-H. DNA-methylation analysis correlated with the transcription data and indicated the induction of epigenetic changes in *Gipr*$^{-/-}$ mice in muscle for *Cpt1b* and *Ppara* once they are exposed to a HFD during IU/L. EMSA experiments suggest a functional relevance of the identified *Ppara* CpG_{-140} site for transcriptional regulation.

It has been shown that the *intra uterine* milieu is able to induce epigenetic changes. A study in rats demonstrated that a HFD during IU/L resulted in DNA-hypomethylation in liver in young male offspring that seemed to be associated with long-term hepatic dysfunction (32).

Miyawaki et al. reported no differences in food intake between WT and *Gipr*$^{-/-}$ mice on a HFD over a period of four days (5). We clearly see an increased cumulative food intake in KO C-C-H compared to WT C-C-H which matches the observation that *Gipr*$^{-/-}$ mice utilize fat for energy metabolism rather than storing it in adipose tissue (5). This phenomenon was reversed when *Gipr*$^{-/-}$ mice were placed on a HFD during IU/L, indicating that GIP physiologically prevents increased energy expenditure in response to increased energy intake as shown earlier (7).

Energy intake is regulated in the hypothalamus and hypothalamic insulin sensitivity is necessary for balanced food consumption (33). It has been shown that a reduction in the catalytic subunit p85α of phosphoinositide 3-kinase (PI3K) enhances insulin stimulated Akt activity (34). It was reported that PI3K subunit p85α was up-regulated in the hypothalamus of mice that were exposed to a HFD throughout IU/L and the first 120 days of life (35). HFD induced obesity was shown to require activation of PI3K dependent hypothalamic pathways (36). Our results indicate that KO C-C-H mice have enhanced hypothalamic insulin sensitivity compared to WT C-C-H mice since we saw a significant reduction of hypothalamic p85α PI3K gene expression in the

former one which correlated with the glucose challenge test. This was reversed in KO H-C-H mice similar to WT C-C-H mice. These results were further supported by increased phosphorylation of the hypothalamic kinase mTOR and S6 protein in the mTOR signaling pathway downstream of Akt. Increased mTOR signaling in the hypothalamus is associated with decreased food intake (37), which was also observed in our study. Thus, central modulation of insulin sensitivity is proposed as a novel mechanism involved in GIP action. However, we could not detect any DNA-methylation changes in the p85α PI3K gene promoter.

In summary, we used the approach of fetal programming by HFD to identify GIP-regulated metabolic pathways which alter hypothalamic insulin sensitivity, the PGC-1α and PPARα driven fat oxidation in skeletal muscle and adipose tissue inflammation.

M. K. designed experiments, researched data, wrote and edited the manuscript and obtained funding supporting the research; F. K. N. researched data, wrote and edited the manuscript; B. N., A. K., E. R. and H. G. designed experiments, researched data, wrote and edited the manuscript; F. I. designed experiments and researched data; T. H. G. and M. O. analyzed data; A. F. H. P. designed experiments, wrote and edited the manuscript and obtained funding supporting the research. A. F. H. P. is the guarantor of this study, has full access to all the data in the study and takes responsibility for the integrity of the data and the accuracy of the data analysis.

ACKNOWLEDGEMENTS

We thank Elisabeth Meyer, Susann Richter, and Kerstin Weinert of the German Institute of Human Nutrition, Nuthetal, Germany and Nicole Spada of the German Research Center for Environmental Health, Neuherberg, Germany, for excellent technical assistance. Dr. Johannes Beckers and Dr. Peter Huypens of the German Research Center for Environmental Health, Neuherberg, Germany, are acknowledged for valuable comments on mouse genetics. Sonja Kunze of the German Research Center for Environmental Health, Neuherberg, Germany, and Dr. Elke Rodriguez and Hans-Jörg Baurecht of the University Hospital, Kiel, Germany, kindly gave advice on methylation analysis. We kindly thank Prof. Bernard Thorens, Dept. of Physiology and Center for Integrative, University of Lausanne, Lausanne, Switzerland for providing the *Gipr*$^{-/-}$ mouse model.

This work was supported by a grant of the Deutsche Forschungsgemeinschaft Pf 164/14-2 to A. F. H. P. and a grant of the Deutsche Diabetes Gesellschaft to M. K.

No conflicts of interest relevant to this study were reported.

REFERENCES

1. Baggio LL, Drucker DJ: Biology of incretins: GLP-1 and GIP. Gastroenterology 2007;132:2131-2157
2. Yip RG, Wolfe MM: GIP biology and fat metabolism. Life Sci 2000;66:91-103
3. Kim SJ, Nian C, McIntosh CH: Activation of lipoprotein lipase by glucose-dependent insulinotropic polypeptide in adipocytes. A role for a protein kinase B, LKB1, and AMP-activated protein kinase cascade. J Biol Chem 2007;282:8557-8567
4. Gogebakan O, Andres J, Biedasek K, Mai K, Kuhnen P, Krude H, Isken F, Rudovich N, Osterhoff MA, Kintscher U, Nauck M, Pfeiffer AF, Spranger J: Glucose-dependent insulinotropic polypeptide reduces fat-specific expression and activity of 11beta-hydroxysteroid dehydrogenase type 1 and inhibits release of free fatty acids. Diabetes 2012;61:292-300
5. Miyawaki K, Yamada Y, Ban N, Ihara Y, Tsukiyama K, Zhou H, Fujimoto S, Oku A, Tsuda K, Toyokuni S, Hiai H, Mizunoya W, Fushiki T, Holst JJ, Makino M, Tashita A, Kobara Y, Tsubamoto Y, Jinnouchi T, Jomori T, Seino Y: Inhibition of gastric inhibitory polypeptide signaling prevents obesity. Nat Med 2002;8:738-742
6. Isken F, Pfeiffer AF, Nogueiras R, Osterhoff MA, Ristow M, Thorens B, Tschop MH, Weickert MO: Deficiency of glucose-dependent insulinotropic polypeptide receptor prevents ovariectomy-induced obesity in mice. Am J Physiol Endocrinol Metab 2008;295:E350-355
7. Isken F, Weickert MO, Tschop MH, Nogueiras R, Mohlig M, Abdelrahman A, Klaus S, Thorens B, Pfeiffer AF: Metabolic effects of diets differing in glycaemic index depend on age and endogenous glucose-dependent insulinotrophic polypeptide in mice. Diabetologia 2009;52:2159-2168
8. Hansotia T, Maida A, Flock G, Yamada Y, Tsukiyama K, Seino Y, Drucker DJ: Extrapancreatic incretin receptors modulate glucose homeostasis, body weight, and energy expenditure. J Clin Invest 2007;117:143-152
9. Warner MJ, Ozanne SE: Mechanisms involved in the developmental programming of adulthood disease. Biochem J 2010;427:333-347
10. Alfaradhi MZ, Ozanne SE: Developmental programming in response to maternal overnutrition. Front Genet 2011;2:27
11. Swenne I, Crace CJ, Milner RD: Persistent impairment of insulin secretory response to glucose in adult rats after limited period of protein-calorie malnutrition early in life. Diabetes 1987;36:454-458
12. Armitage JA, Taylor PD, Poston L: Experimental models of developmental programming: consequences of exposure to an energy rich diet during development. J Physiol 2005;565:3-8
13. Samuelsson AM, Matthews PA, Argenton M, Christie MR, McConnell JM, Jansen EH, Piersma AH, Ozanne SE, Twinn DF, Remacle C, Rowlerson A, Poston L, Taylor PD: Diet-induced obesity in female mice leads to offspring hyperphagia, adiposity, hypertension, and insulin resistance: a novel murine model of developmental programming. Hypertension 2008;51:383-392
14. Oben JA, Mouralidarane A, Samuelsson AM, Matthews PJ, Morgan ML, McKee C, Soeda J, Fernandez-Twinn DS, Martin-Gronert MS, Ozanne SE, Sigala B, Novelli M, Poston L, Taylor PD: Maternal obesity during pregnancy and lactation programs the development of offspring non-alcoholic fatty liver disease in mice. J Hepatol 2010;52:913-920

15. Kruse M, Seki Y, Vuguin PM, Du XQ, Fiallo A, Glenn AS, Singer S, Breuhahn K, Katz EB, Charron MJ: High-fat intake during pregnancy and lactation exacerbates high-fat diet-induced complications in male offspring in mice. Endocrinology 2013;154:3565-3576
16. Burdge GC, Hanson MA, Slater-Jefferies JL, Lillycrop KA: Epigenetic regulation of transcription: a mechanism for inducing variations in phenotype (fetal programming) by differences in nutrition during early life? Br J Nutr 2007;97:1036-1046
17. Ristow M, Mulder H, Pomplun D, Schulz TJ, Muller-Schmehl K, Krause A, Fex M, Puccio H, Muller J, Isken F, Spranger J, Muller-Wieland D, Magnuson MA, Mohlig M, Koenig M, Pfeiffer AF: Frataxin deficiency in pancreatic islets causes diabetes due to loss of beta cell mass. J Clin Invest 2003;112:527-534
18. Hartil K, Vuguin PM, Kruse M, Schmuel E, Fiallo A, Vargas C, Warner MJ, Durand JL, Jelicks LA, Charron MJ: Maternal substrate utilization programs the development of the metabolic syndrome in male mice exposed to high fat in utero. Pediatr Res 2009;66:368-373
19. Ranalletta M, Du XQ, Seki Y, Glenn AS, Kruse M, Fiallo A, Estrada I, Tsao TS, Stenbit AE, Katz EB, Charron MJ: Hepatic response to restoration of GLUT4 in skeletal muscle of GLUT4 null mice. Am J Physiol Endocrinol Metab 2007;293:E1178-1187
20. Ehrich M, Nelson MR, Stanssens P, Zabeau M, Liloglou T, Xinarianos G, Cantor CR, Field JK, van den Boom D: Quantitative high-throughput analysis of DNA methylation patterns by base-specific cleavage and mass spectrometry. Proc Natl Acad Sci U S A 2005;102:15785-15790
21. Zeilinger S, Kuhnel B, Klopp N, Baurecht H, Kleinschmidt A, Gieger C, Weidinger S, Lattka E, Adamski J, Peters A, Strauch K, Waldenberger M, Illig T: Tobacco smoking leads to extensive genome-wide changes in DNA methylation. PLoS One 2013;8:e63812
22. Goossens GH: The role of adipose tissue dysfunction in the pathogenesis of obesity-related insulin resistance. Physiol Behav 2008;94:206-218
23. Song DH, Getty-Kaushik L, Tseng E, Simon J, Corkey BE, Wolfe MM: Glucose-dependent insulinotropic polypeptide enhances adipocyte development and glucose uptake in part through Akt activation. Gastroenterology 2007;133:1796-1805
24. Naitoh R, Miyawaki K, Harada N, Mizunoya W, Toyoda K, Fushiki T, Yamada Y, Seino Y, Inagaki N: Inhibition of GIP signaling modulates adiponectin levels under high-fat diet in mice. Biochem Biophys Res Commun 2008;376:21-25
25. Trayhurn P: Endocrine and signalling role of adipose tissue: new perspectives on fat. Acta Physiol Scand 2005;184:285-293
26. Weisberg SP, McCann D, Desai M, Rosenbaum M, Leibel RL, Ferrante AW, Jr.: Obesity is associated with macrophage accumulation in adipose tissue. J Clin Invest 2003;112:1796-1808
27. Oh da Y, Morinaga H, Talukdar S, Bae EJ, Olefsky JM: Increased macrophage migration into adipose tissue in obese mice. Diabetes 2012;61:346-354
28. Sell H, Eckel J: Chemotactic cytokines, obesity and type 2 diabetes: in vivo and in vitro evidence for a possible causal correlation? Proc Nutr Soc 2009;68:378-384
29. Rausch ME, Weisberg S, Vardhana P, Tortoriello DV: Obesity in C57BL/6J mice is characterized by adipose tissue hypoxia and cytotoxic T-cell infiltration. Int J Obes (Lond) 2008;32:451-463
30. Usdin TB, Mezey E, Button DC, Brownstein MJ, Bonner TI: Gastric inhibitory polypeptide receptor, a member of the secretin-vasoactive intestinal peptide receptor family, is widely distributed in peripheral organs and the brain. Endocrinology 1993;133:2861-2870
31. Zhou H, Yamada Y, Tsukiyama K, Miyawaki K, Hosokawa M, Nagashima K, Toyoda K, Naitoh R, Mizunoya W, Fushiki T, Kadowaki T, Seino Y: Gastric inhibitory polypeptide

modulates adiposity and fat oxidation under diminished insulin action. Biochem Biophys Res Commun 2005;335:937-942
32. Dudley KJ, Sloboda DM, Connor KL, Beltrand J, Vickers MH: Offspring of mothers fed a high fat diet display hepatic cell cycle inhibition and associated changes in gene expression and DNA methylation. PLoS One 2011;6:e21662
33. Sharma MD, Garber AJ, Farmer JA: Role of insulin signaling in maintaining energy homeostasis. Endocr Pract 2008;14:373-380
34. Mauvais-Jarvis F, Ueki K, Fruman DA, Hirshman MF, Sakamoto K, Goodyear LJ, Iannacone M, Accili D, Cantley LC, Kahn CR: Reduced expression of the murine p85alpha subunit of phosphoinositide 3-kinase improves insulin signaling and ameliorates diabetes. J Clin Invest 2002;109:141-149
35. Page KC, Malik RE, Ripple JA, Anday EK: Maternal and postweaning diet interaction alters hypothalamic gene expression and modulates response to a high-fat diet in male offspring. Am J Physiol Regul Integr Comp Physiol 2009;297:R1049-1057
36. Klockener T, Hess S, Belgardt BF, Paeger L, Verhagen LA, Husch A, Sohn JW, Hampel B, Dhillon H, Zigman JM, Lowell BB, Williams KW, Elmquist JK, Horvath TL, Kloppenburg P, Bruning JC: High-fat feeding promotes obesity via insulin receptor/PI3K-dependent inhibition of SF-1 VMH neurons. Nat Neurosci 2011;14:911-918
37. Cota D, Proulx K, Smith KA, Kozma SC, Thomas G, Woods SC, Seeley RJ: Hypothalamic mTOR signaling regulates food intake. Science 2006;312:927-930

Fasted serum metabolites

	WT C-C-H	KO C-C-H	KO H-C-H
Blood glucose (mg/dl)	167±9	118±12¶,$	160±11
Insulin (ng/ml)	4.28±0.32	2.17±0.21*	3.58±0.64
Cholesterol (mmol/l)	5.22±0.26	3.33±0.33§	4.44±0.40
Triglycerides (mmol/l)	0.98±0.04	0.88±0.08	0.92±0.04
NEFA (mmol/l)	0.86±0.03	0.86±0.06	0.83±0.03

Table 1: Fasted glucose, insulin, total cholesterol, triglycerides and non-esterified fatty acids (NEFA) serum levels at 45 weeks of age (20 weeks on HFD). *P<0.05 compared to WT C-C-H, ¶P<0.01 compared to WT C-C-H, §P<0.005 compared to WT C-C-H, $P<0.05 compared to KO H-C-H; n= 4-13 per group.

FIGURE LEGENDS

Figure 1: Schematic representation of the study. Open bars indicate periods of food exposition with a regular rodent chow, hatched bars indicate periods of food exposition with a high fat diet. HFD: High fat diet; NMR: Nuclear magnetic resonance spectroscopy; GTT: *Intra peritoneal* glucose tolerance test; WT: Wild type offspring; KO: *Gipr*$^{-/-}$ offspring. Exposure to either a regular rodent chow (C) or a high fat diet (H) during pregnancy and lactation results in three different experimental groups (WT C-C-H, KO C-C-H and KO H-C-H): The first letter indicates the diet during pregnancy and lactation, the second letter indicates the diet post weaning up to the age of 25 weeks and the third letter indicates the diet during the last 20 weeks of life (until the age of 45 weeks).

Figure 2: Body weight, adiposity and energy intake. **A**: Growth curve of offspring from 4 weeks until 23 weeks of age on a standard rodent chow. Except for week 4, 13, and 14 there was no significant difference in body weight. WT C-C: Wild type offspring exposed to a regular chow during pregnancy/ lactation and post weaning; KO C-C: *Gipr*$^{-/-}$ offspring exposed to a regular chow during pregnancy/ lactation and post weaning; KO H-C: *Gipr*$^{-/-}$ offspring exposed to a HFD during pregnancy/ lactation and switched to a regular diet post weaning. *P<0.05 for KO H-C compared to KO C-C. **B**: Growth curve of offspring after a HFD was started at 25 weeks of age. WT C-C-H gained significantly more weight compared to KO C-C-H. Body weight of KO H-C-H is in range between the two other groups. **C**: Adiposity was measured by nuclear magnetic resonance spectroscopy. KO H-C-H had significantly increased body fat compared to KO C-C-H after 12 weeks on a HFD and KO C-C-H had significantly lower body fat compared to WT C-C-H. **D**: Cumulative energy intake is shown for selected time points. After a HFD was fed, WT C-

C-H and KO H-C-H had similar cumulative food intake which was lower compared to KO C-C-H. *P<0.05, **P<0.01, ***P<0.005; n= 4-13 per group.

Figure 3: Glucose tolerance test at 43 weeks of age (18 weeks on HFD). After an overnight fast, mice received an i.p. injection of 2.0 g glucose per kg body weight. **A**: KO C-C-H had significantly improved glucose tolerance compared to WT C-C-H and KO H-C-H. $ P<0.01 for KO C-C-H vs.WT C-C-H and P<0.05 for KO C-C H vs. KO H-C-H, # P<0.05 for KO C-C-H vs.WT C-C-H and for KO C-C-H vs. KO H-C-H. **B**: AUC: Area under the curve for glucose, *P<0.05. KO H-C-H showed higher glucose levels compared to KO C-C-H although insulin levels were not significantly different. **C**: Plasma insulin levels, * P<0.05, ** P<0.01, *** P<0.001 for WT C-C-H vs. KO C-C-H. **D**: AUC: Area under the curve for insulin. n=4-13 per group.

Figure 4: Adipocyte cell size was determined in H&E stained sections of epididymal white adipose tissue. **A**: KO C-C-H had significantly smaller adipocytes compared to WT C-C-H and KO H-C-H, ***P<0.005, n=4-13 per group. **B:** Histogram of the distribution of cell sizes. Representative image of adipocyte size of (**C**) WT C-C-H, (**D**) KO C-C-H and (**E**) KO H-C-H.

Figure 5: Gene expression levels in epididymal adipose tissue (**A**) and in gastrocnemius muscle (**B**). *Ccl2*: Macrophage chemoattractant protein-1, *Ccl3*: Macrophage inflammatory protein-1α, *Emr1*: F4/80, marker of macrophage infiltration, *Il6*: Interleukin-6, *Tnf*: Tumor necrosis factor-α, *Cd36*: Cluster of differation 36 fatty acid transporter, *Lpl*: Lipoprotein lipase, *Ppara*: Peroxisome proliferator-activated receptor α, *Ppargc1a*: Peroxisome proliferator-activated receptor gamma coactivator 1-α, *Cpt1a*: Carnitine palmitoyltransferase-1 α, *Cpt1b*: Carnitine

palmitoyltransferase-1 β, *Acadm*: Medium-chain acyl-CoA dehydrogenase, *Acadl*: Long-chain acyl-CoA dehydrogenase. *P<0.05, **P<0.01, n=4-13 per group.

Figure 6: A: Gene expression levels in hypothalamus of phosphatidylinositol 3-kinase catalytic subunit p110 (*Pik3ca*), phosphatidylinositol 3-kinase regulatory subunit p85α (*Pik3r1*), signal transducer and activator of transcription 3 (*Stat3*) and neuropeptide Y receptor 1 (*Npy1r*). **B:** Analysis of hypothalamic protein phosphorylation of Akt (Thr308), Akt(Ser473), AMPKa (Thr172), S6 Ribosomal Protein (Ser235/236), mTOR (Ser2448), p70 S6 Kinase (Thr389). *P<0.05, **P<0.01, n=4-13 per group.

Figure 7: DNA-methylation of CpG-sites of the *Cpt1b* (**A**, **B**, **C**) and *Ppara* (**D**) promoter and their correlation with gene expression levels in muscle. DNA-Methylation of CpG-sites is expressed in percent (%). A negative Spearman correlation coefficient (r) indicates inverse correlation between DNA-methylation of the CpG-site and gene expression. **E:** Methylation specific formation of a protein-DNA complex in the *Ppara* promoter region in mouse myoblasts. Methylated (m) and unmethylated (um) Cy5-labelled probes carrying the Ppara CpG_{-140} site, were investigated in competition EMSA using C2C12 mouse myoblast nuclear extracts. Lane 1 and 2 represent oligonucleotides without incubation with nuclear extract. Lane 3 and 10 represent protein-DNA complex formation at the unmethylated and methylated CpG. In lane 4, 5, 11, 12 competition with unlabeled methylated oligonucleotides was performed, whereas in lane 6, 7, 13, 14 competition with unlabeled unmethylated oligonucleotides was performed. Specificity was assured by competition experiments with unlabeled NfkB consensus oligonucleotides (lanes 8, 9, 15, 16). Arrow (c) indicates methylation specific binding. n=4-13 per group.

FIG. 1

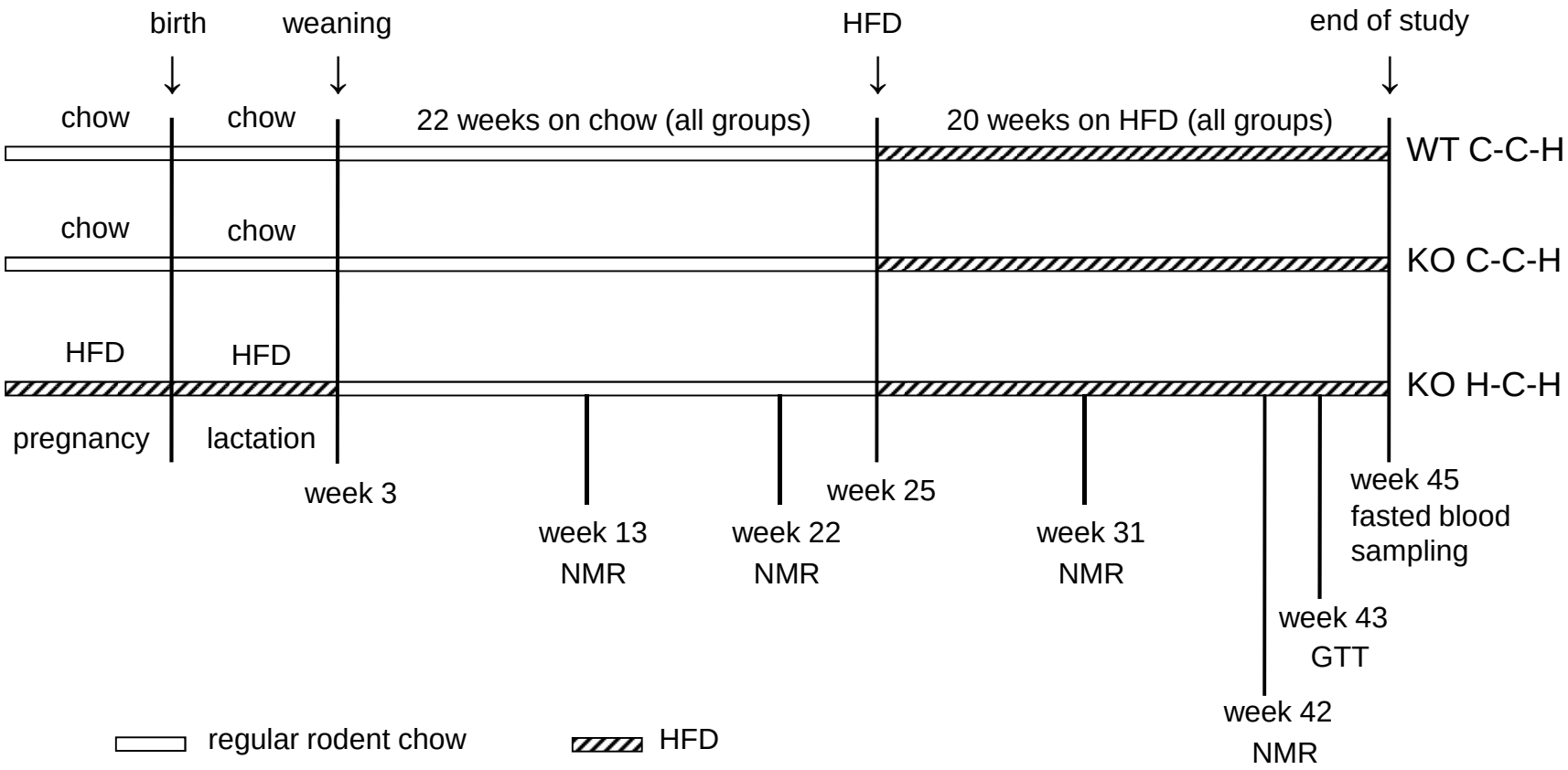
birth
weaning
HFD
end of study
chow
chow
22 weeks on chow (all groups)
20 weeks on HFD (all groups)
WT C-C-H
chow
chow
KO C-C-H
HFD
HFD
KO H-C-H
pregnancy
lactation
week 3
week 13
NMR
week 22
NMR
week 25
week 31
NMR
week 42
NMR
week 43
GTT
week 45
fasted blood
sampling
regular rodent chow
HFD

FIG. 2

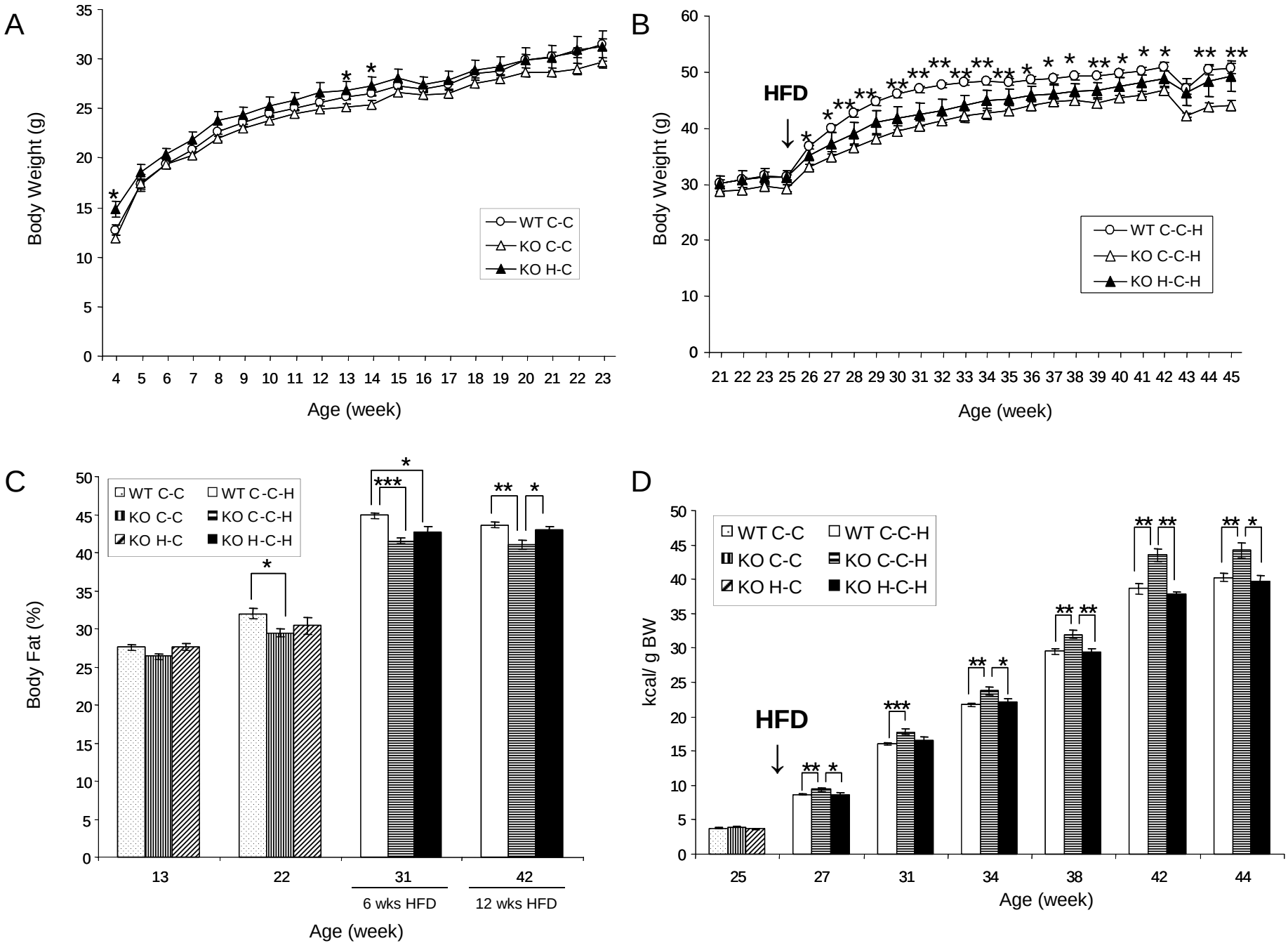
A
Body Weight (g)
Age (week)
WT C-C
KO C-C
KO H-C
B
HFD
Body Weight (g)
Age (week)
WT C-C-H
KO C-C-H
KO H-C-H
C
Body Fat (%)
WT C-C
WT C-C-H
KO C-C
KO C-C-H
KO H-C
KO H-C-H
6 wks HFD
12 wks HFD
Age (week)
D
kcal/ g BW
HFD
Age (week)

FIG. 3

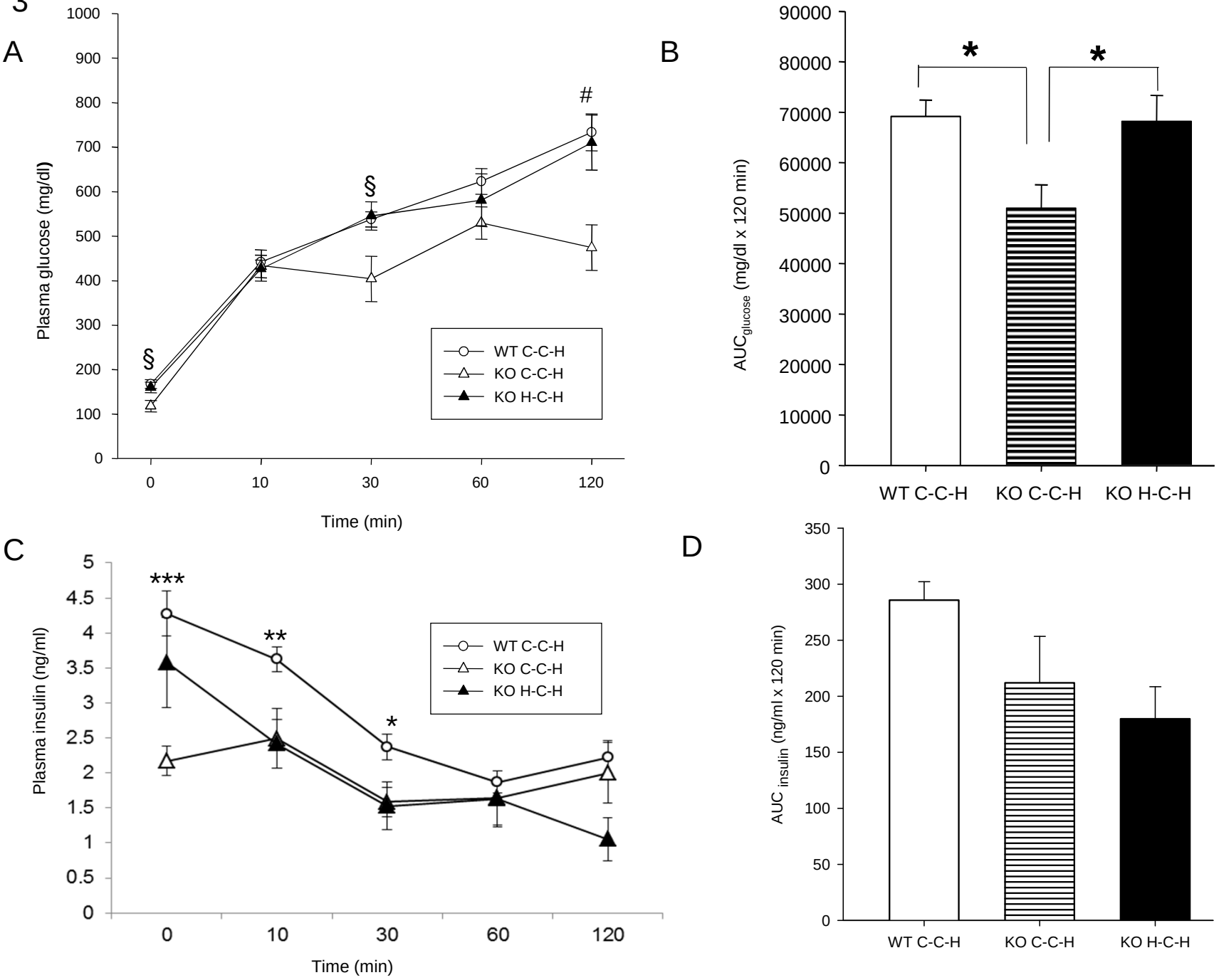
A
Plasma glucose (mg/dl)
Time (min)
WT C-C-H
KO C-C-H
KO H-C-H
§
§
#
B
AUC glucose (mg/dl x 120 min)
WT C-C-H
KO C-C-H
KO H-C-H
*
*
C
Plasma insulin (ng/ml)
Time (min)
WT C-C-H
KO C-C-H
KO H-C-H
***
**
*
D
AUC insulin (ng/ml x 120 min)
WT C-C-H
KO C-C-H
KO H-C-H

FIG. 4

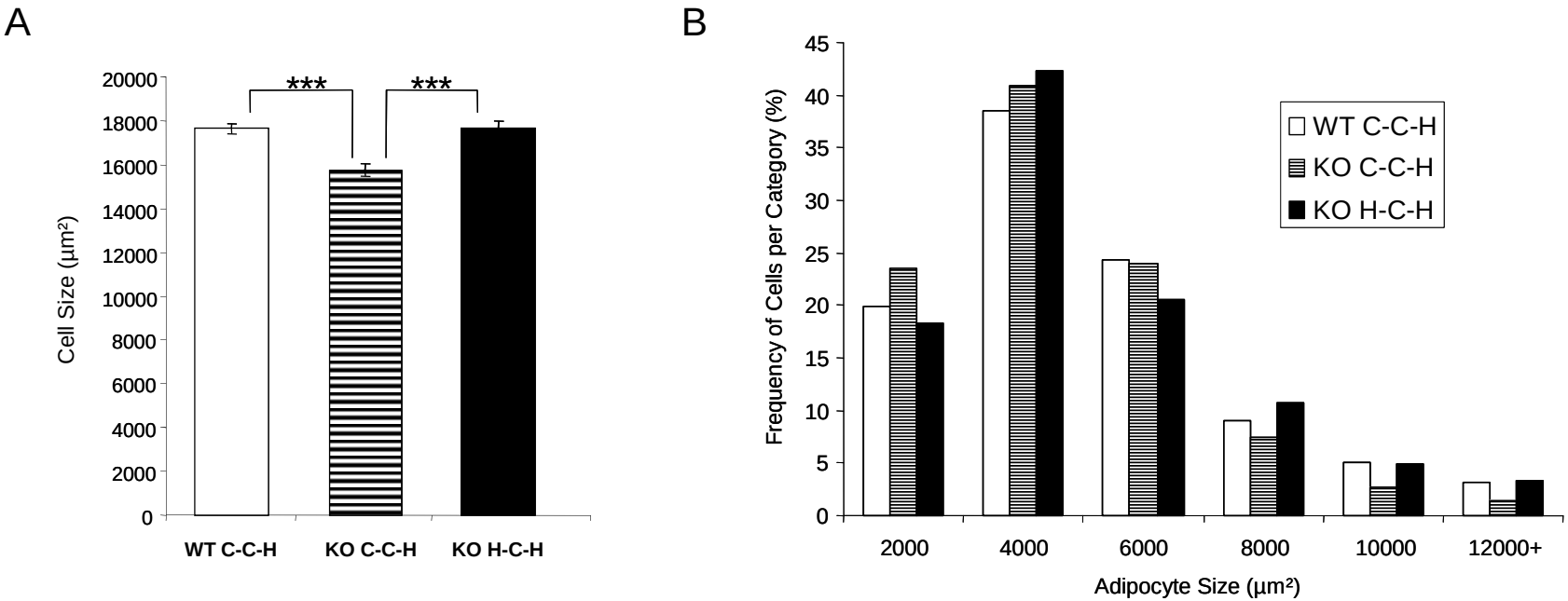
A
***
***
Cell Size (µm²)
20000
18000
16000
14000
12000
10000
8000
6000
4000
2000
0
WT C-C-H
KO C-C-H
KO H-C-H
B
Frequency of Cells per Category (%)
45
40
35
30
25
20
15
10
5
0
WT C-C-H
KO C-C-H
KO H-C-H
2000
4000
6000
8000
10000
12000+
Adipocyte Size (µm²)
C
WT C-C-H
D
KO C-C-H
E
KO H-C-H

FIG. 5

A: Adipose Tissue

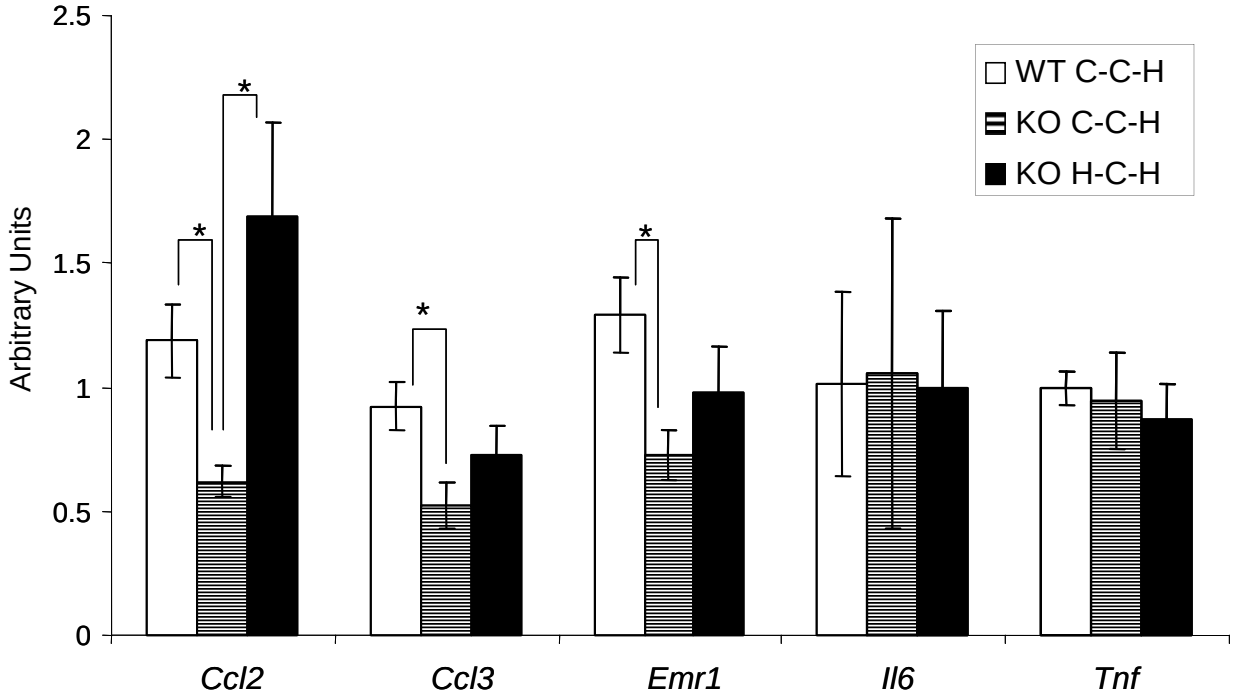

B: Skeletal Muscle

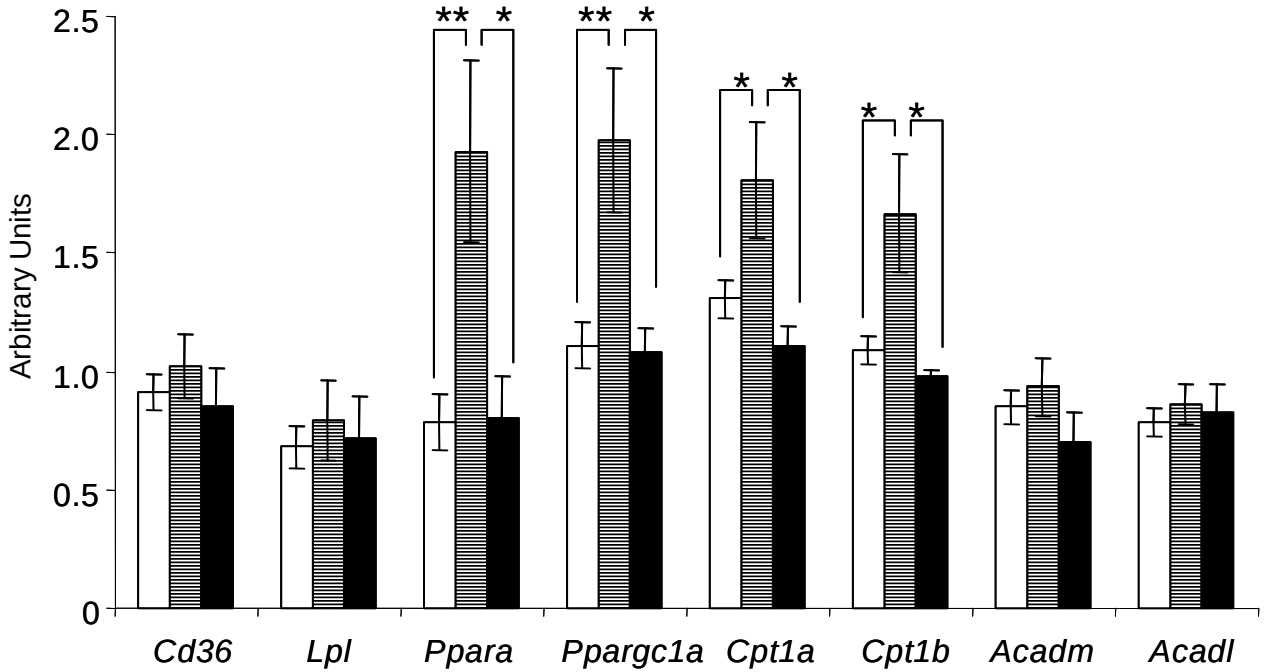

FIG. 6

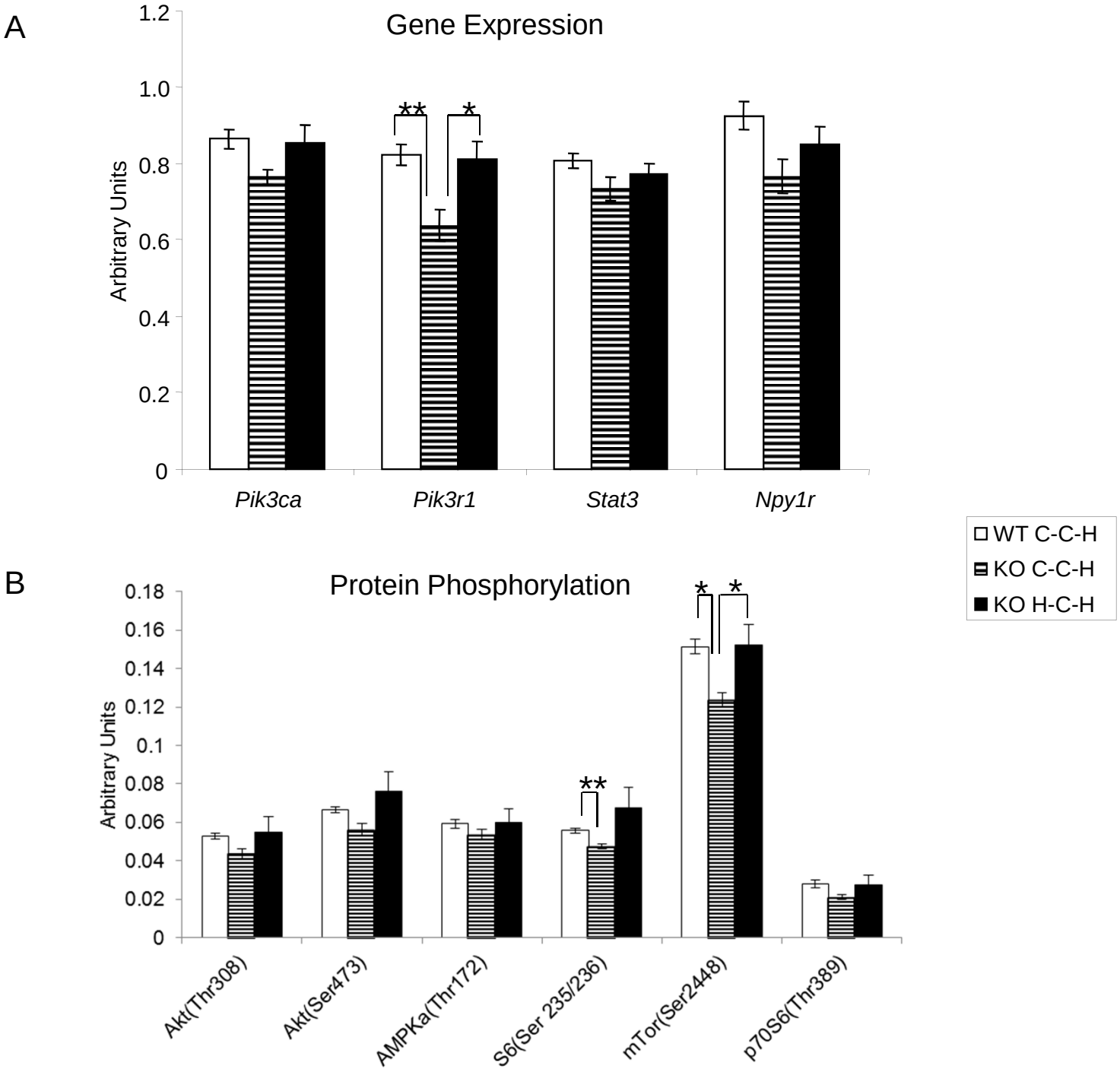
A
Gene Expression
Arbitrary Units
1.2
1.0
0.8
0.6
0.4
0.2
0
**
*
Pik3ca
Pik3r1
Stat3
Npy1r
WT C-C-H
KO C-C-H
KO H-C-H
B
Protein Phosphorylation
Arbitrary Units
0.18
0.16
0.14
0.12
0.1
0.08
0.06
0.04
0.02
0
*
*
**
Akt(Thr308)
Akt(Ser473)
AMPKa(Thr172)
S6(Ser 235/236)
mTor(Ser2448)
p70S6(Thr389)

FIG. 7

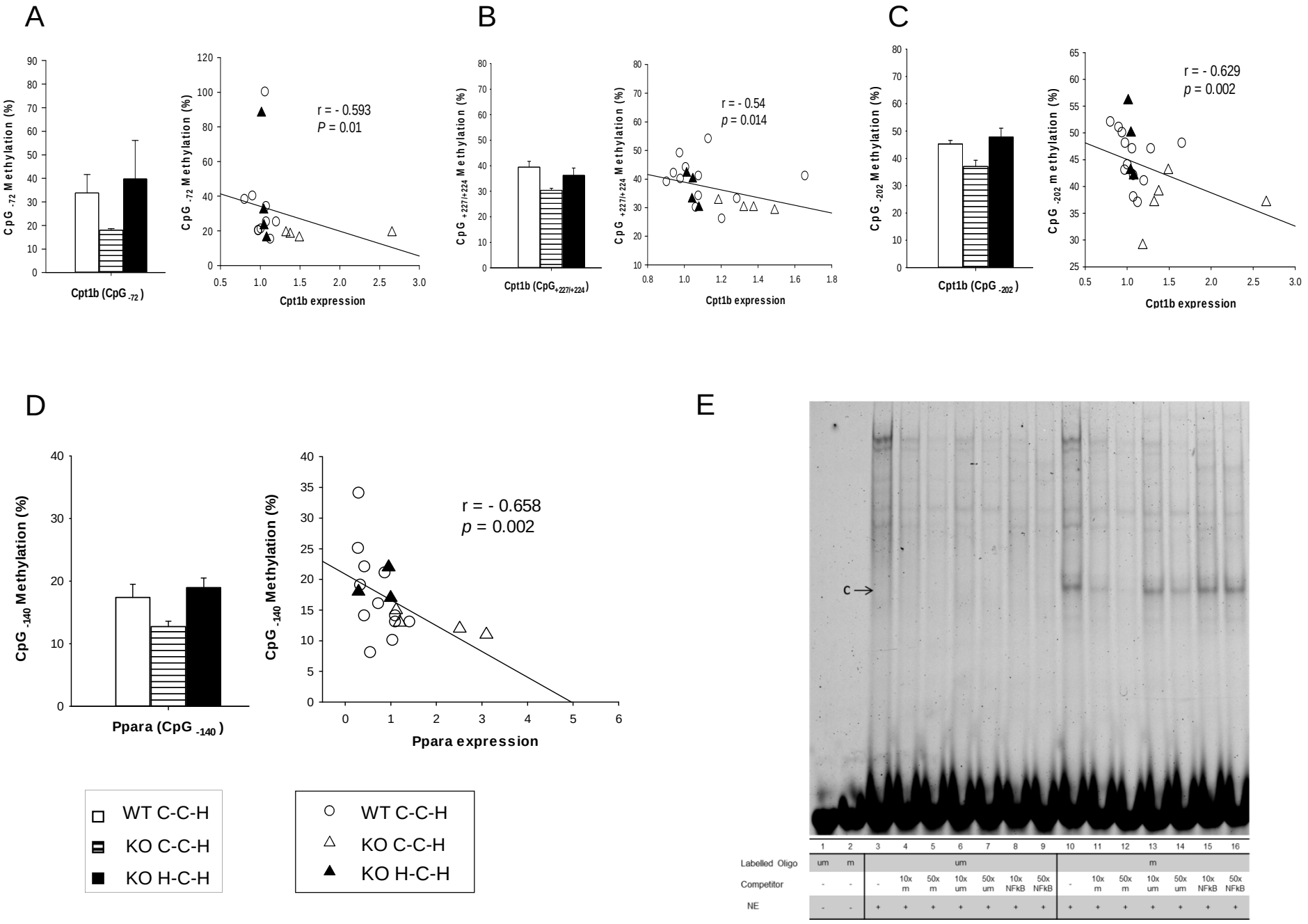
A
CpG -72 Methylation (%)
Cpt1b (CpG -72)
r = - 0.593
P = 0.01
Cpt1b expression
B
CpG +227/+224 Methylation (%)
Cpt1b (CpG +227/+224)
r = - 0.54
p = 0.014
Cpt1b expression
C
CpG -202 Methylation (%)
Cpt1b (CpG -202)
r = - 0.629
p = 0.002
Cpt1b expression
D
CpG -140 Methylation (%)
Ppara (CpG -140)
r = - 0.658
p = 0.002
Ppara expression
WT C-C-H
KO C-C-H
KO H-C-H
WT C-C-H
KO C-C-H
KO H-C-H
E
C
1 2 3 4 5 6 7 8 9 10 11 12 13 14 15 16
Labelled Oligo um m um m
Competitor - - - 10x m 50x m 10x um 50x um 10x NFkB 50x NFkB - 10x m 50x m 10x um 50x um 10x NFkB 50x NFkB
NE - - + + + + + + + + + + + + + +

Supplementary Table 1: Primer sequences used for quantitative real time PCR analysis.

Gene	Forward Primer	Reverse Primer	Gene Bank
Acadl	GGCTTGCTTGGCATCAACA	CGCAGAGAAACATGG	NM_007381.3
Acadm	AGAGCTCTAGACGAAGCCACGA	GAGTTCAACCTTCATCGCCATT	NM_007382.4
Agrp	CCCAGGTCTAAGTCTGAATGGC	TTCTGTGGATCTAGCACCTCCG	NM_007427.2
Cart	AACGCATTCCGATCTACGAGA	ACAGTCACACAGCTTCCCGAT	NM_013732.6
Ccl2	TCTCTCTTCCTCCACCACCATG	GCGTTAACTGCATCTGGCTGA	NM_011333.3
Ccl3	GCGGCTGATGATTGGACAA	ATCTCCAGCTCGAGCAATGG	NM_011337.2
Cnr1	GGCACCTCTTTCTCAGTCACGT	GGTGATGGTACGGAAGGTGGTA	NM_007726.3
Cd36	GGACATACTTAGATGTGGAACCCATA	TGTTGACCTGCAGTCGTTTTG	NM_001159558.1
Cpt1a	CACCAACGGGCTCATCTTCT	CCTTCTATCGAATTTGCTCTGGTT	NM_013495.2
Cpt1b	TGGGACTGGTCGATTGCAT	AGTGGCCATACCTTTCCGG	NM_009948.2
Crh	ATTTCACACACGCAGTCGGTAT	AAGCCCAGGAATGAAGTCCA	NM_205769.2
Emr1	GGATGGATAATGGCTGCTGGT	CCAGGCAAGGAGGACAGAGTTT	NM_010130.4
Hprt	CAGTCCCAGCGTCGTGATTA	AGCAAGTCTTTCAGTCCTGTC	NM_013556
Il6	TCTGCAAGAGACTTCCATCCAGT	TGTCACCAGCATCAGTCCCA	NM_031168.1
Lepr	CGGAGAGCCACGCAACTT	CAGCCCCGGGCAGTTT	NM_146146.2
Lpl	GGACTGAGGATGGCAAGCAA	GCCACTGTGCCGTACAGAGA	NM_008509.2
Mch	TTCAAAGAACACAGGCTCCAAA	ACTCAGCATTCTGAACTCCATTCTC	NM_029971.2
Npy	ACTCCGCTCTGCGACACTACAT	GCGTTTTCTGTGCTTTCCTTCA	NM_023456.2
Npy1r	CTGCAGTATTTCGGCCCACTCT	ACTGTCCCGGATCTTGTCCATC	NM_010934
Pik3ca	ACCTCAGGCTTGAAGAGTGTCG	CCGTAAGTCGTCGCCATTTTTA	NM_008839.2
Pik3r1	AACCGAAACAAAGCGGAGAA	TTGACTTCGCCGTCTACCACT	NM_001024955.1
Pomc	GCCACTGAACATCTTTGTCCC	AATCTCGGCATCTTCCACGT	NM_008895.3
Ppara	GTCACACAATGCAATTCGCTTT	TTTGCTTTTTCAGATCTTGGCA	NM_011144.6
Ppargc1c	ACAGCCGTAGGCCCAGGTAC	GCCTTTCGTGCTCATAGGCTT	NM_008904.2
Stat3	ATCTGTGTGACACCAACGACCT	TCAGCACCTTCACCGTTATTTC	NM_213659.2
Tnf	ATGAGAAGTTCCCAAATGGCCT	GGGTCTGGGCCATAGAACTGA	NM_013693.2
Trh	GTGCCAACCAAGACAAGGAT	TTCTTCCCAGCTTCTTTGGA	NM_009426.2

Supplementary Table 2: Sequences of PCR primers used for EpiTYPER methylation analysis and product size of each amplicon.

Amplicon	Primer	Sequence	Product size (bp)
Ppara_#3	forward	aggaagagagGGTAGAGTTTTAGTGTTTGAGTTGGA	491
	reverse	cagtaatacgactcactatagggagaaggctATAAAAAAACTACCCAAAATCACCC	
Ppara_#4	forward	aggaagagagGGGTGATTTTGGGTAGTTTTTTTAT	445
	reverse	cagtaatacgactcactatagggagaaggctCCAACCCCTAAACACCTAAAACT	
Ppara_#7	forward	aggaagagagTGTAGTTTTAGGTGTTTAGGGGTTG	491
	reverse	cagtaatacgactcactatagggagaaggctAAATCAATCTATCAAAAAACCTCCA	
Pik3r1_#1	forward	aggaagagagGTAGTTTTTGTTTTTGGGAAGGAA	346
	reverse	cagtaatacgactcactatagggagaaggctACCAAACTAAACCATAATAATCCCC	
Pik3r1_#8	forward	aggaagagagGGGGATTATTATGGTTTAGTTTGG	354
	reverse	cagtaatacgactcactatagggagaaggctAACAAACTACCAACTCCCAAT	
Pik3r1_#9	forward	aggaagagagGATTGGGAGTTGGTAGTTTGT	183
	reverse	cagtaatacgactcactatagggagaaggctTAAAACCCAAACTAAACAAAAAAAA	
Pik3r1_#10	forward	aggaagagagTTTTTTTTGTTTAGTTTGGGTTTTA	358
	reverse	cagtaatacgactcactatagggagaaggctAACTCCTAAACCTTAATAACCCTCC	
Pik3r1_#11	forward	aggaagagagGGGAGGGTTATTAAGGTTTAGGAG	385
	reverse	cagtaatacgactcactatagggagaaggctACAAACAAAACCAAAAATTACAAAA	
Ppargc1a_#1	forward	aggaagagagTTTATGTTATTTTATATAGAGTTTTGGTTG	356
	reverse	cagtaatacgactcactatagggagaaggctAACCAAATATTTCCTTTTCTTTCTTC	
Ppargc1a_#3	forward	aggaagagagAAGTTATTAAAAAGTAGGTTGGGTTGTT	489
	reverse	cagtaatacgactcactatagggagaaggctCCTTCAAACACTCCTCTAATAAAAAAA	
Ppargc1a_#4	forward	aggaagagagTTTTATTATTGTTTATGGTGTTTGGTT	373
	reverse	cagtaatacgactcactatagggagaaggctAAAATCCCTCCTTTCAATAATTCTA	
Cpt1b_#1	forward	aggaagagagAGTGAATTGGAAAGTTATTGTTTGG	408
	reverse	cagtaatacgactcactatagggagaaggctATACTAAAACCACTCCCTTCCCTAA	
Cpt1b_#8	forward	aggaagagagTTAGGGAAGGGAGTGGTTTTAGTAT	266
	reverse	cagtaatacgactcactatagggagaaggctTTCTCCACCCCAATTTAAAAATAA	
Cpt1b_#10	forward	aggaagagagTTTGGTTTTTTTGGTTTATGTTTTT	462
	reverse	cagtaatacgactcactatagggagaaggctAATCTCCTATCCCATAATACTCCCTAA	
Cpt1b_#12	forward	aggaagagagAAGTAAATTTGAGTTGTGAGTTGGG	488
	reverse	cagtaatacgactcactatagggagaaggctCCATCCTAAAATTTATTCAACACCT	
Cpt1b_#22	forward	aggaagagagGTTGGAGTAGTAGTGGTTTTTGAGG	416
	reverse	cagtaatacgactcactatagggagaaggctCCTATACTAATCCCCAACTCACAAC	
Cpt1a_#5	forward	aggaagagagGAAAGATGGAGGTAAATAGGGTTTT	482
	reverse	cagtaatacgactcactatagggagaaggctCCAAAAACCAACACACTCATAATC	
Cpt1a_#7	forward	aggaagagagGAGATTATGAGTGTGTTGGTTTTTG	364
	reverse	cagtaatacgactcactatagggagaaggctTTCCTTACCCTAAAAACCTCAATTT	
Cpt1a_#15	forward	aggaagagagGGTTTTTAGGGTAAGGAATGTTGTT	383
	reverse	cagtaatacgactcactatagggagaaggctAAAAAAAATACCCTCTACTTCTCCA	

Supplementary Table 3: Sequences of oligonucleotide used for EMSA

Name	Primer	Sequence
CG_Cpt1b+227,+224	forward	AAGCCTGGCCAACCGCCGCTGCCACCGAACC
CG_Cpt1b+227,+224	reverse	GGTTCGGTGGCAGCGGCGGTTGGCCAGGCTT
F_CG_Cpt1b+227,+224	competition	AAGCCTGGCCAACCGCCGCTGCCACCGAACC
(me)CG_Cpt1b+227,+224	forward	AAGCCTGGCCAAC-(me)CGC-(me)CGCTGCCACCGAACC
(me)CG_Cpt1b+227,+224	reverse	GGTTCGGTGGCAG-(me)CGG-(me)CGGTTGGCCAGGCTT
F_(me)CG_Cpt1b+227,+224	competition	AAGCCTGGCCAAC-(me)CGC-(me)CGCTGCCACCGAACC
CG_Cpt1b-72	forward	GGCCCATGTCCCCACGTCCTTCAGGCCTGG
CG_Cpt1b-72	reverse	CCAGGCCTGAAGGACGTGGGGACATGGGCC
F_CG_Cpt1b-72	competition	GGCCCATGTCCCCACGTCCTTCAGGCCTGG
(me)CG_Cpt1b-72	forward	GGCCCATGTCCCCA-(me)CGTCCTTCAGGCCTGG
(me)CG_Cpt1b-72	reverse	CCAGGCCTGAAGGA-(me)CGTGGGGACATGGGCC
F_(me)CG_Cpt1b-72	competition	GGCCCATGTCCCCA-(me)CGTCCTTCAGGCCTGG
CG_Cpt1b-202	forward	TCCTTTTGGGGGAGCGCCTAGGGAGGGTGG
CG_Cpt1b-202	reverse	CCACCCTCCCTAGGCGCTCCCCCAAAAGGA
F_CG_Cpt1b-202	competition	TCCTTTTGGGGGAGCGCCTAGGGAGGGTGG
(me)CG_Cpt1b-202	forward	TCCTTTTGGGGGAG-(me)CGCCTAGGGAGGGTGG
(me)CG_Cpt1b-202	reverse	CCACCCTCCCTAGG-(me)CGCTCCCCCAAAAGGA
F_(me)CG_Cpt1b-202	competition	TCCTTTTGGGGGAG-(me)CGCCTAGGGAGGGTGG
CG_Ppara-140	forward	TGGCCCTGCGGACCCGCAGGCGGAGTGCAG
CG_Ppara-140	reverse	CTGCACTCCGCCTGCGGGTCCGCAGGGCCA
F_CG_Ppara-140	competition	TGGCCCTGCGGACCCGCAGGCGGAGTGCAG
(me)CG_Ppara-140	forward	TGGCCCTGCGGACC-(me)CGCAGGCGGAGTGCAG
(me)CG_Ppara-140	reverse	CTGCACTCCGCCTG-(me)CGGGTCCGCAGGGCCA
F_(me)CG_Ppara-140	competition	TGGCCCTGCGGACC-(me)CGCAGGCGGAGTGCAG
Oct1	forward	TGTCGAATGCAAATCACTAGAA
Oct1	reverse	TTCTAGTGATTTGCATTCGACA
NFkB	forward	AGTTGAGGGGACTTTCCCAGGC
NFkB	reverse	GCCTGGGAAAGTCCCCTCAACT

Supplementary Figure 1: Crown-like structures (CLS) in white adipose tissue. Tissues were stained with an F4/80 anti-mouse antibody. Crown-like structures were determined in three randomly chosen areas within the slides. Slightly fewer CLS were observed in KO C-C-H compared to WT C-C-H and KO H-C-H, respectively. However, this was not statistically significant (**D**). n=4-13 per group. CLS: Crown-like structure, WAT: White adipose tissue.

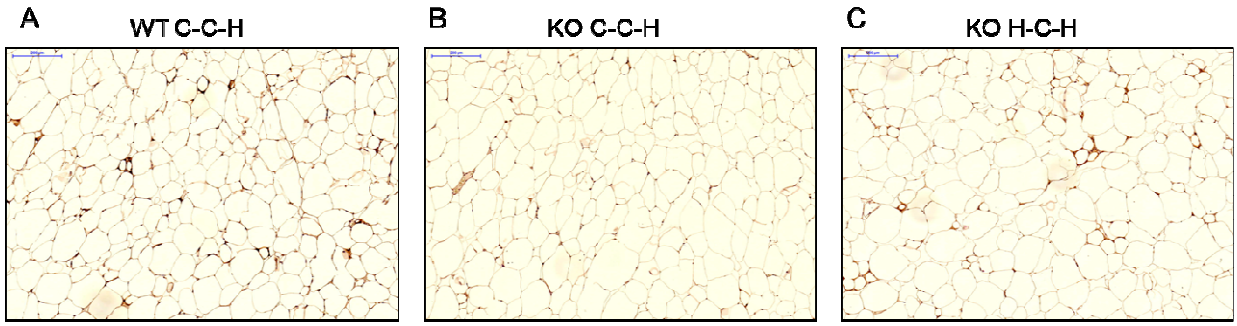

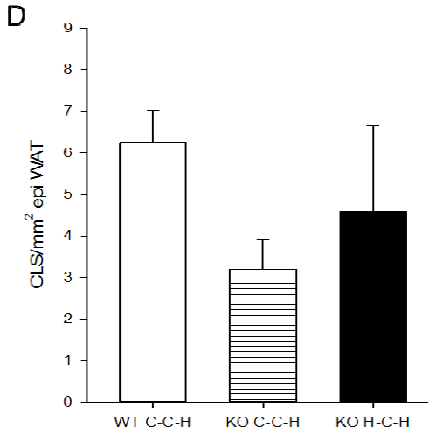

Supplementary Figure 2. Gene expression levels in hypothalamus of leptin receptor – long form (LEPR), proopiomelanocortin (POMC), corticotropin releasing hormone (CRH), thyrotropin-releasing hormone (TRH), cocaine and amphetamine-regulated transcript (CART), melanin-concentrating hormone (MCH), agouti-related protein (AgRP), neuropeptide Y (NPY), cannabinoid receptor 1 (CNR1) and suppressor of cytokine signaling 3 (SOCS3). *P<0.05, n=4-13 per group.

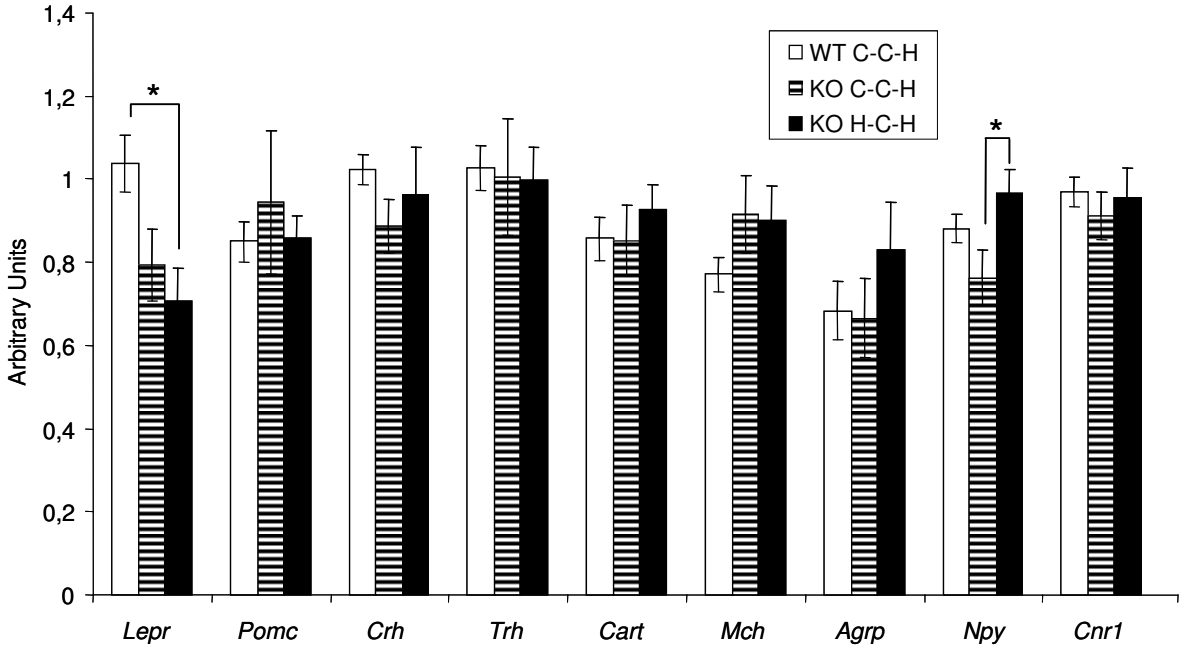

Supplementary Figure 3: No methylation specific formation of a protein-DNA complex at the Cpt1b CpG_{-72} site in mouse C2C12 myoblasts. Methylated (m) and unmethylated (um) Cy5-labelled probes carrying the CpG_{-72} site, were investigated in competition EMSAs using C2C12 mouse myoblast nuclear extracts. Lane 1 and 2 represent oligonucleotides without incubation with nuclear extract. Lane 3 and 10 represent protein-DNA complex formation at the unmethylated and methylated CpG. In lane 4, 5, 13, 14 competition with unlabeled methylated oligonucleotides was performed, whereas in lane 6, 7, 11, 12 competition with unlabeled unmethylated oligonucleotides was performed. Specificity was assured by competition experiments with unlabeled Oct1/NfKB consensus oligonucleotides (lanes 8, 9, 15, 16).

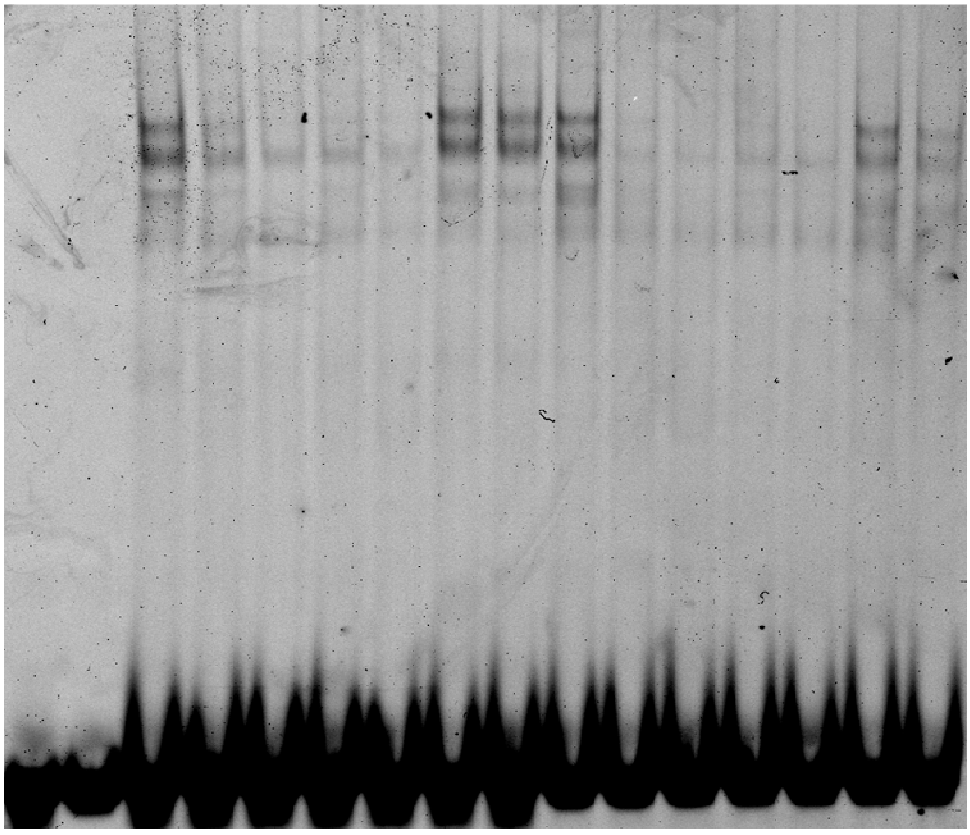

	1	2	3	4	5	6	7	8	9	10	11	12	13	14	15	16
Labelled Oligo	um	m				um							m			
Competitor	-	-	-	10x m	50x m	10x um	50x um	10x NFkB	50x NFkB	-	10x um	50x um	10x m	50x m	10x NFkB	50x NFkB
NE	-	-	+	+	+	+	+	-	+	+	+	+	+	+	+	+

Supplementary Figure 4: No methylation specific formation of a protein-DNA complex at the Cpt1b $CpG_{+227/+224}$ site in mouse C2C12 myoblasts. Methylated (m) and unmethylated (um) Cy5-labelled probes carrying the $CpG_{+227/+224}$ site, were investigated in competition EMSAs using C2C12 mouse myoblast nuclear extracts. Lane 1 and 2 represent oligonucleotides without incubation with nuclear extract. Lane 3 and 10 represent protein-DNA complex formation at the unmethylated and methylated CpG. In lane 4, 5, 13, 14 competition with unlabeled methylated oligonucleotides was performed, whereas in lane 6, 7, 11, 12 competition with unlabeled unmethylated oligonucleotides was performed. Specificity was assured by competition experiments with unlabeled Oct1/NfKB consensus oligonucleotides (lanes 8, 9, 15, 16).

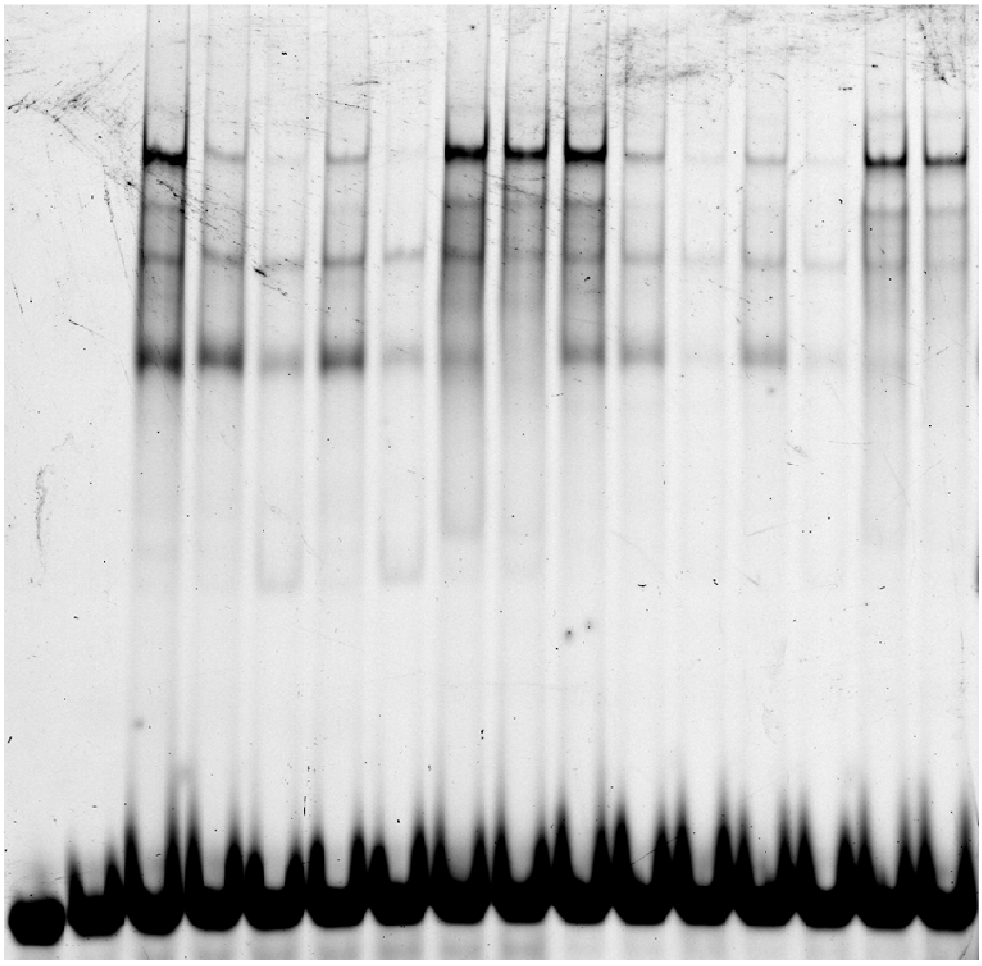

	1	2	3	4	5	6	7	8	9	10	11	12	13	14	15	16
Labelled Oligo	um	m				um							m			
Competitor	-	-	-	10x m	50x m	10x um	50x um	10x Oct1	50x Oct1	-	10x um	50x um	10x m	50x m	10x Oct1	50x Oct1
NF	-	-	+	+	+	+	+	-	+	+	+	+	+	+	+	+

Supplementary Figure 5: No methylation specific formation of a protein-DNA complex at the Cpt1b CpG_{-202} site in mouse C2C12 myoblasts. Methylated (m) and unmethylated (um) Cy5-labelled probes carrying the CpG_{-202} site, were investigated in competition EMSAs using C2C12 mouse myoblast nuclear extracts. Lane 1 and 2 represent oligonucleotides without incubation with nuclear extract. Lane 3 and 10 represent protein-DNA complex formation at the unmethylated and methylated CpG. In lane 4, 5, 13, 14 competition with unlabeled methylated oligonucleotides was performed, whereas in lane 6, 7, 11, 12 competition with unlabeled unmethylated oligonucleotides was performed. Specificity was assured by competition experiments with unlabeled Oct1/NfKB consensus oligonucleotides (lanes 8, 9, 15, 16).

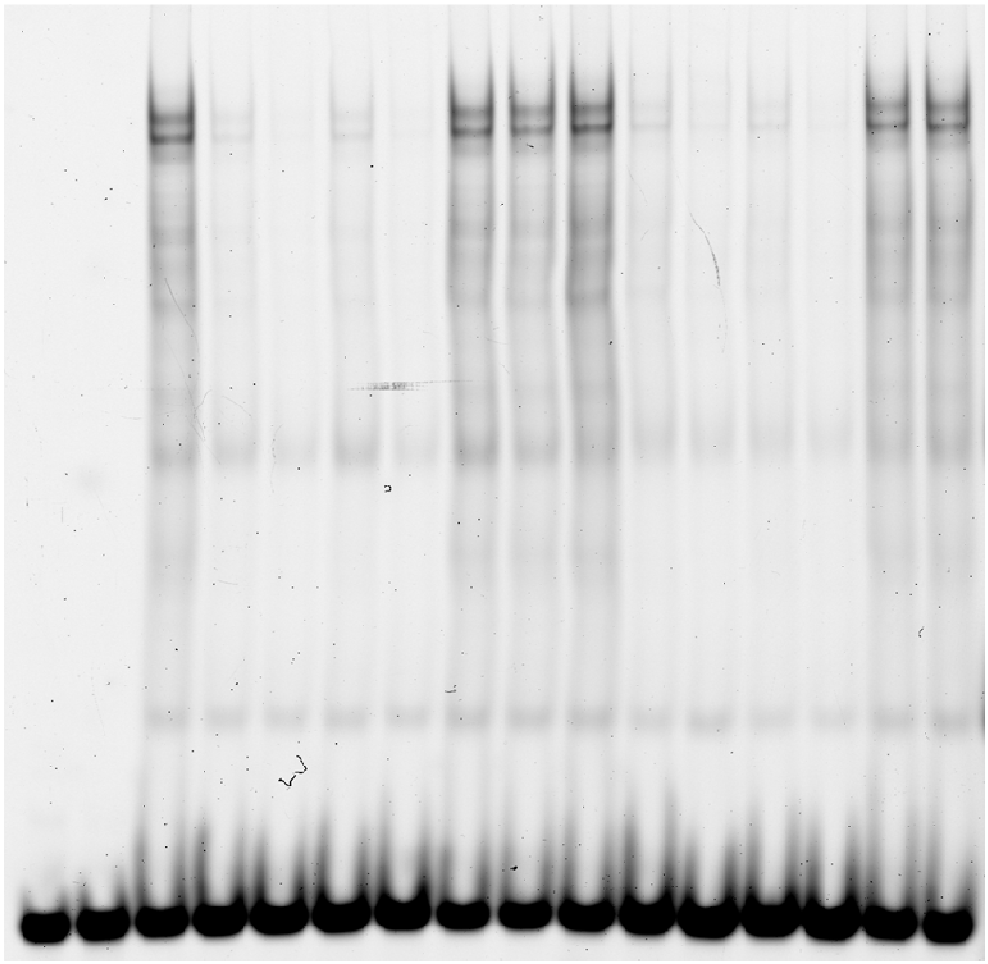

	1	2	3	4	5	6	7	8	9	10	11	12	13	14	15	16
Labelled Oligo	um	m				um							m			
Competitor	-	-	-	10x m	50x m	10x um	50x um	10x Oct1	50x Oct1	-	10x um	50x um	10x m	50x m	10x Oct1	50x Oct1
NE	-	-	+	+	+	+	+	-	+	+	+	+	+	+	+	+

Supplementary Figure 6: Schematic representation of the study including an additional group of wild type mice that received a high fat diet during pregnancy and lactation and between week 25 and 45 of life (WT H-C-H). Open bars indicate periods of food exposition with a regular rodent chow, hatched bars indicate periods of food exposition with a high fat diet. HFD: High fat diet; NMR: Nuclear magnetic resonance spectroscopy; GTT: Intra peritoneal glucose tolerance test; WT: Wild type offspring; KO: *Gipr*$^{-/-}$ offspring. For further details see also Figure 1 in the main text.
Results of key experiments of the study with these for groups are shown in Supplementary Figures 7-11. A two-way ANOVA analysis with genotype and maternal diet as the independent variables was performed. Significance was accepted at $P<0.05$.

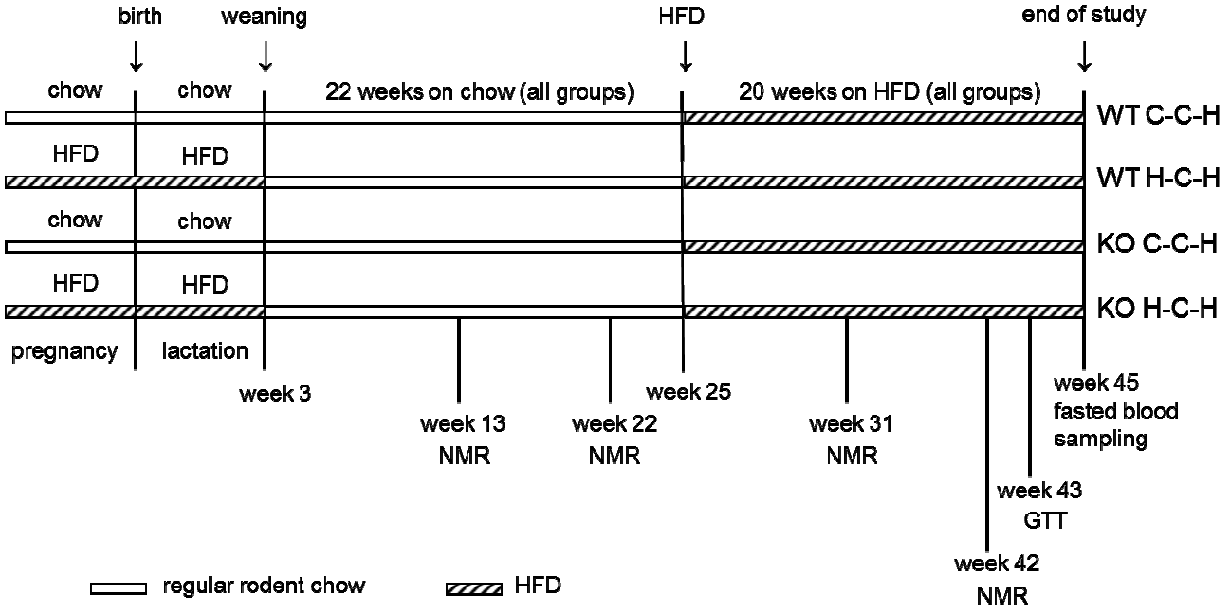

Supplementary Figure 7: A: Growth curve of offspring from 4 weeks until 23 weeks of age on a standard rodent chow. WT C-C: Wild type offspring exposed to a regular chow during pregnancy/ lactation and post weaning; WT H-C: Wild type offspring exposed to HFD during pregnancy/ lactation and post weaning; KO C-C: *Gipr*$^{-/-}$ offspring exposed to a regular chow during pregnancy/ lactation and post weaning; KO H-C: *Gipr*$^{-/-}$ offspring exposed to a HFD during pregnancy/ lactation and switched to a regular diet post weaning; n= 3-13 per group, a = two-way ANOVA P<0.05 for maternal diet, b = two-way ANOVA P<0.05 for interaction genotype x maternal diet.
B: Growth curve of offspring after a HFD was started at 25 weeks of age; n= 3-13 per group, for WT H-C-H n= 2 for week 42-45, c = two-way ANOVA P<0.05 for genotype, d = two-way ANOVA P<0.01 for genotype, e = two-way ANOVA P<0.05 for interaction genotype x maternal diet.

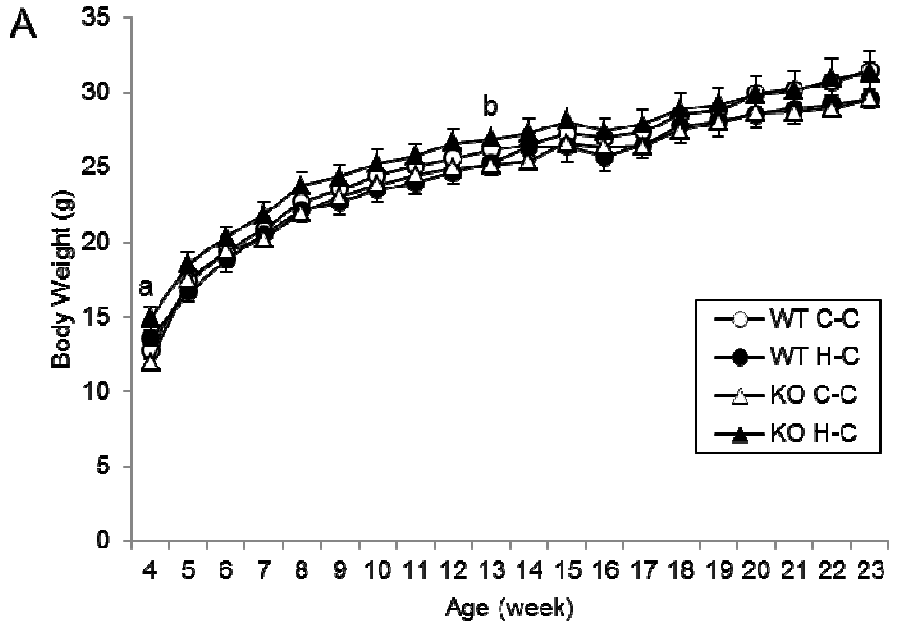

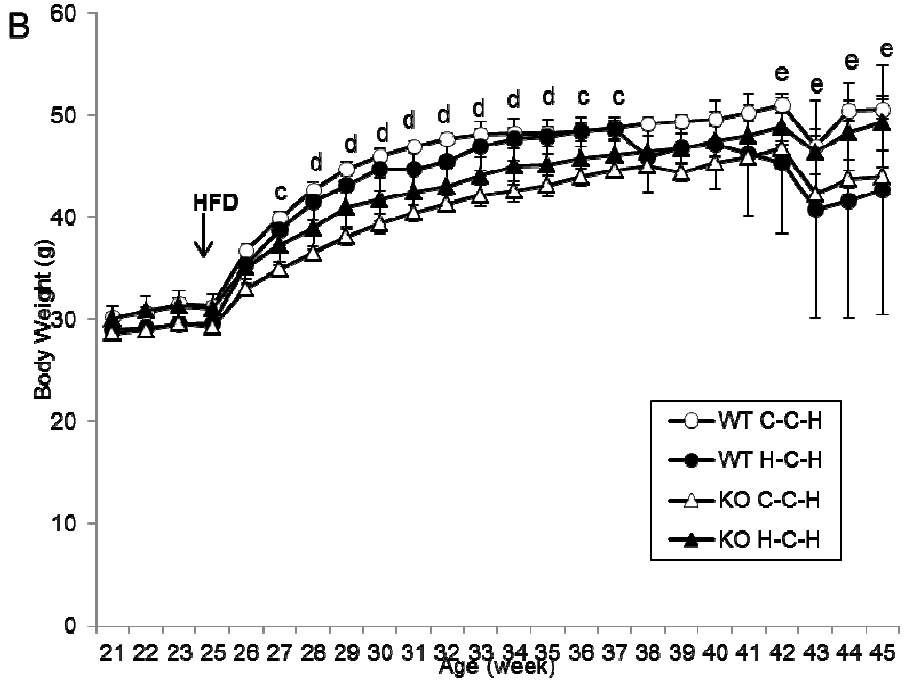

Supplementary Figure 8: Adiposity was measured by nuclear magnetic resonance spectroscopy, n= 3-13 per group, for WT H-C-H n=2 at week 42. Two-way ANOVA: P<0.001 for genotype at 31 weeks and P<0.01 for interaction genotype x maternal diet at 42 weeks.

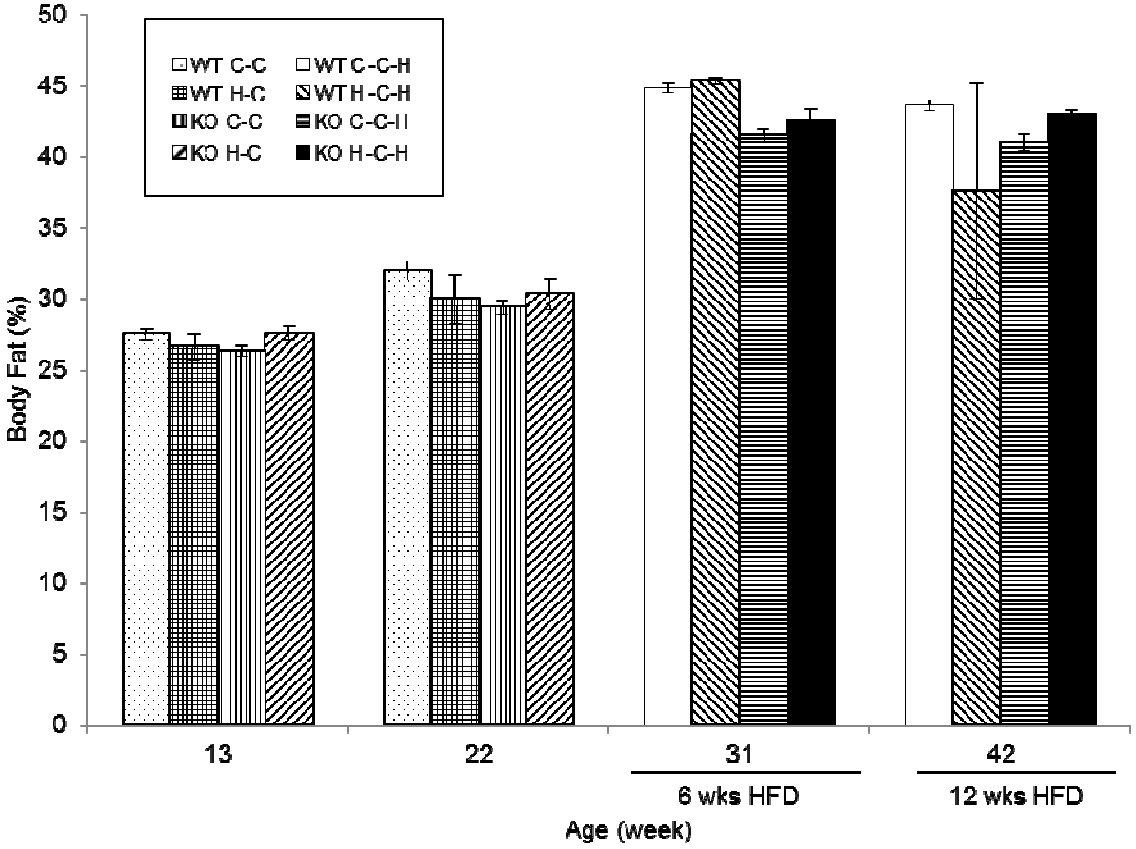

Supplementary Figure 9: Glucose tolerance test at 43 weeks of age (18 weeks on HFD). After an overnight fast, mice received an i.p. injection of 2.0 g glucose per kg body weight. **A:** Plasma glucose levels. **B:** AUC: Area under the curve for glucose, two-way ANOVA: P<0.05 for interaction genotype x maternal diet. **C:** Plasma insulin levels. **D:** AUC: Area under the curve for insulin, two-way ANOVA: P<0.05 for maternal diet.
n=3-13 per group, a = two-way ANOVA P<0.05 for maternal diet, b = two-way ANOVA P<0.05 for interaction genotype x maternal diet, c = two-way ANOVA P<0.01 for interaction genotype x maternal diet.

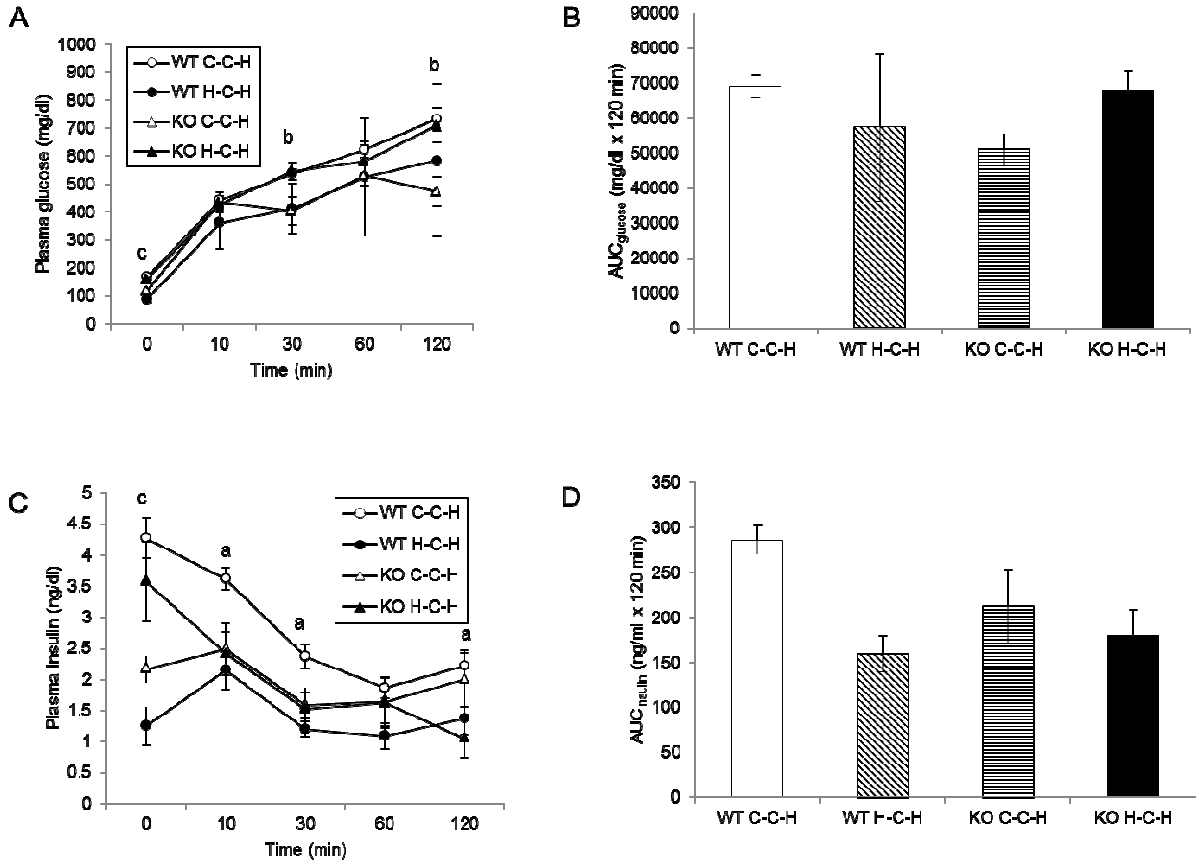

Supplementary Figure 10: Gene expression levels in gastrocnemius muscle. *Cd36*: Cluster of differation 36 fatty acid transporter, *Lpl*: Lipoprotein lipase, *Ppara*: Peroxisome proliferator-activated receptor α, *Ppargc1a*: Peroxisome proliferator-activated receptor gamma coactivator 1-α, *Cpt1a*: Carnitine palmitoyltransferase-1 α, *Cpt1b*: Carnitine palmitoyltransferase-1 β, *Acadm*: Medium-chain acyl-CoA dehydrogenase, *Acadl*: Long-chain acyl-CoA dehydrogenase. n=4-13 per group; n=2 for WT H-C-H.
Two-way ANOVA: *Ppara*: P<0.05 for interaction genotype x maternal diet. *Ppargc1a*: P<0.05 for genotype and for maternal diet. *Cpt1a*: P<0.01 for genotype, P<0.001 for maternal diet and P<0.01 for interaction genotype x maternal diet. *Cpt1b*: P<0.01 for interaction genotype x maternal diet.

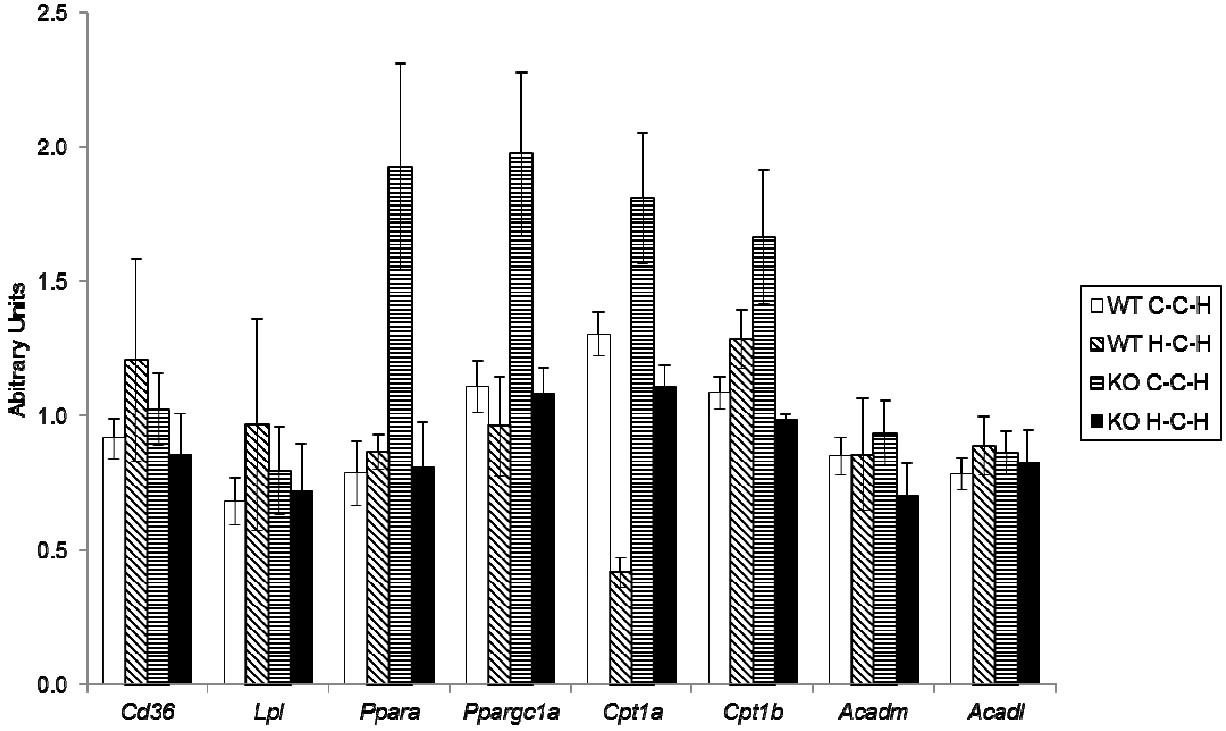

Supplementary Figure 11: Gene expression levels in hypothalamus of phosphatidylinositol 3-kinase catalytic subunit p110 (*Pik3ca)*, phosphatidylinositol 3-kinase regulatory subunit p85α *(Pik3r1*), signal transducer and activator of transcription 3 (*Stat3*) and neuropeptide Y receptor 1 *(Npy1r*). n=4-13 per group; n=2 for WT H-C-H.
Two-way ANOVA: *Pik3r1*: P<0.05 for genotype and for maternal diet.